AN UPDATED STRONG-MOTION DATABASE OF TÜRKIYE WITH AN AUTOMATIC DATA PROCESSING ALGORITHM

OTOMATİK VERİ İŞLEME ALGORİTMASI İLE GÜNCELLENMİŞ TÜRKİYE KUVVETLİ YER HAREKETİ VERİ TABANI

BARAN GÜRYUVA

Assoc. Prof. MUSTAFA ABDULLAH SANDIKKAYA

Supervisor

ASSOC. PROF. ÖZKAN KALE

Co-supervisor

Submitted to

Graduate School of Science and Engineering of Hacettepe University

as a Partial Fulfilment to the Requirements

for the Award of the Degree of Master of Science

in Civil Engineering

September 2023

i

ii

ABSTRACT

AN UPDATED STRONG-MOTION DATABASE OF TÜRKIYE WITH AN AUTOMATIC DATA PROCESSING ALGORITHM

Baran GÜRYUVA

Master of Science, Civil Engineering

Supervisor: Assoc. Prof. M. Abdullah Sandıkkaya

Co-supervisor: Assoc. Prof. Özkan Kale

September 2023, 56 pages

The earthquake strong-motion database of Türkiye (SMD-TR) is the updated version of the dataset that is initially compiled by Akkar et al. (2010). The updated dataset is composed of 9244 earthquakes of magnitudes $3.0 \leq M \leq 7.8$ that occurred between 1976 and 2023. It includes 95890 three-component waveforms recorded at 1,022 stations (55375 records are processed). The database includes event metadata compiled from national and international seismological agencies as well as literature. Events were classified according to their tectonic environments (i.e., active crustal and subduction) and the aftershocks were flagged. The station information provided by AFAD was used to compute the main site parameters, including time-based average of shear-wave velocity of uppermost 30 m (V_{S30}) and depth-to-rock horizon at which the shear wave-velocity (V_S) attains 1 km/s (Z1). Necessary finite-fault distance metrics were calculated and records with hanging wall effects were flagged, as well as pulse-like records. An automatic processing scheme was developed to determine the waveform quality, apply appropriate filters to remove low- and high-frequency noise, and compute ground motion

iii

parameters. The automatic processing was applied to small magnitude (M<5.5) events whereas manual processing scheme is preferred for waveforms recorded from larger events (M≥5.5). The peak ground motion values, spectral ordinates, and ground-motion duration are provided along with the key data processing parameters in the flatfile.

Keywords: ground-motion prediction models, ground-motion processing, seismic hazard, strong-motion database.

ÖZET

OTOMATİK VERİ İŞLEME ALGORİTMASI İLE GÜNCELLENMİŞ TÜRKİYE KUVVETLİ YER HAREKETİ VERİ TABANI

Baran GÜRYUVA

Yüksek Lisans, İnşaat Mühendisliği Bölümü

Tez Danışmanı: Doç. Dr. Mustafa Abdullah Sandıkkaya

Eş Danışman: Doç. Dr. Özkan Kale

Eylül 2023, 56 sayfa

Türkiye Kuvvetli Yer Hareketi Veri Tabanı (SMD-TR), Akkar vd. (2010) tarafından derlenen veri tabanının güncellenmiş halidir. Güncellenen veri seti, 1976 ile Şubat 2023 arasında meydana gelen $3.0 \leq M \leq 7.8$ büyüklüğündeki 9244 depremden oluşmaktadır. Bu veri tabanında, 1,022 istasyonda kaydedilen 95,890 üç bileşenli dalga formları (55,375 filtrelenmiş kayıt) bulunmaktadır. Veri tabanı, ulusal ve uluslararası sismoloji kurumlarından ve literatürden derlenen deprem meta verilerini içermektedir. Deprem tektonik yapılarına göre sınıflandırılmış (aktif kabuk ve dalma - batma) ve artçı şok olan depremleri belirlenmiştir. AFAD tarafından sağlanan istasyon bilgileri kullanılarak, zeminin üst 30 metresindeki zamana dayalı ortalama kayma dalgası hızı (V_{S30}) ve anakayaya ($V_{S30} = 1km/s$) olan derinlik (Z1) dahil olmak üzere zemin parametrelerini hesaplanmıştır. Ayrıca, kaynak-fay mesafe metriklerini hesaplanmış, tavan ve taban bloğu ve atımlı kayıtları işaretlenmiştir. Kayıtların kalitesini belirlemek, uygun filtrelerle düşük ve yüksek frekanslı gürültüyü arındırmak ve yer hareketi parametrelerini hesaplamak için otomatik bir işleme algoritması geliştirilmiştir. Otomatik işleme küçük magnitüddeki (M<5.5) depremlere uygulanırken, daha büyük depremlerden (M≥5.5)

toplanan kayıtlar için manuel işleme şemasını tercih edilmiştir. Maksimum yer hareketi değerleri, spektral parametreler ve yer hareketi süresi veri tabanında, veri işleme parametreleriyle birlikte sunulmaktadır.

Anahtar Kelimeler: kuvvetli yer hareketi veri tabanı, sismik tehlike, yer hareketi işlenmesi, yer hareketi tahmin denklemleri

ACKNOWLEDGEMENTS

TABLE OF CONTENTS

LIST OF FIGURES

LIST OF TABLES

SYMBOLS AND ABBREVIATIONS

Symbols

f_a	Theoretical source spectrum (Atkinson and Silva, 2000)
f_{hc}	High-cut filter frequency
f_{lc}	Low-cut filter frequency
$f_{Nyquist}$	Nyquist frequency
M_d	Duration magnitude
M_L	Local magnitude
M_W	Moment magnitude
R_{epi}	Epicentral distance
R_{hyp}	Hypocentral distance
R_{JB}	Joyner-Boore distance
R_{rup}	Nearest distance to the fault rupture plane itself
R_X	Distance perpendicular to the fault strike from the surface projection of the up-dip edge of the fault plane
R_Y	Distance parallel to the fault strike from the midpoint of the surface projection of the fault plane
V_{S30}	Shear wave velocity in the uppermost 30 meters
Z_1	Depth-to-the-rock layer
Z_{tor}	Depth-to-the-top-of rupture
κ	Kappa

Abbreviations

AFAD	Afet ve Acil Durum Yönetimi Başkanlığı
AI	ARIAS Intensity

xiii

APS	Automatic Processing Scheme
BQ	Bad Quality
CAV	Cumulative Absolute Velocity
EAF	Eastern Anatolian Fault
EMME	Earthquake Model of the Middle East
ESM	The pan-European Engineering Strong Motion
ETDC	Early Termination During the Coda
GMPE	Ground Motion Prediction Equations
IDR	Insufficient Digitizer Resolution
ISC-EHB	International Seismological Centre's Engdahl-van der Hilst-Buland Bulletin
ISC-GEM	International Seismological Centre's Global Earthquake Model
ITACA	ITalian ACcelerometric Archive
KOERI	Kandilli Observatory and Earthquake Research Institute
MASW	Multi-Channel Analysis of Surface Waves
MPS	Manuel Processing Scheme
MS	Multiple Shocks
NAF	North Anatolian Fault
NGA-East	Next Generation Attenuation Relations for Central Eastern North-America
NGA-Sub	Next Generation Attenuation for Subduction Zone Regions Project
NGA-West2	Next Generation of Ground-Motion Attenuation Models for Western US, 2
NRPE	Number of Records Per Event
PGA	Peak Ground Acceleration

PGD	Peak Ground Displacement
PGV	Peak Ground Velocity
PSA	Pseudo Spectral Acceleration
RCTC	Rotated Combination of Two Component Ground Motions Calculation
RESORCE	Reference database for Seismic Ground Motion in Europe
SMD-TR	Strong-Motion Database of Türkiye
SNR	Signal to Noise Ratio
SOF	Style of Faulting
S-WT	S-wave Triggered
TADAS	Turkish Acceleometric Database and Analysis System
T-NSMP	Turkish National Strong-Motion Project
TSTHG	Türkiye Sismik Tehlike Haritasının Güncellenmesi
TUBITAK	Türkiye Bilimsel ve Teknolojik Araştırma Kurumu
UDAP	Ulusal Deprem Araştırma Programı

1. INTRODUCTION

Türkiye is located at a high seismic activity region includes many active faults, rendering earthquakes a frequent and formidable natural hazard. In the annals of its history, Türkiye suffered from many large magnitude earthquakes. Particular examples of the seismic events that have occurred within the past 25 years are the Kocaeli and Düzce earthquakes of 1999, Van earthquakes of 2011 and most recently, February 6th, 2023 earthquakes of Pazarcık and Elbistan. These events, marked by their substantial impact, encompassed wide-ranging devastation, pronounced economic ramifications, and the tragic loss of human lives. Consequently, earthquake resistant structures should be built for preservation of both human lifes and property against future devastating earthquakes. In order to achieve this goal a well-studied strong-motion database is needed to generate region specific ground-motion models, as well as assess the other ground-motion models to be used in the seismic hazard analysis.

1.1 Literature Review

Earthquake strong ground-motion databases primarily serve three essential purposes: (i) the development of ground motion prediction models, (ii) the assessment of ground-motion characteristics for hazard analyses, and (iii) the provision of accelerometric data for structural and geotechnical analysis. These databases constitute crucial information sources for ground-motion modeling and analyses and have been established in various seismically active regions worldwide. Notable examples of such well-organized efforts include the work by Russo et al. (ITACA; 2022), Lanzano et al. (ESM; 2021), Scordilis et al. (2018), and Akkar et al. (RESORCE; 2014), which have focused on compiling pan-European strong-motion data. Additionally, there are database projects such as those by Ancheta et al. (NGA-West2; 2014), Contreras et al. (NGA-Sub; 2022), and Goulet et al. (NGA-East; 2018), which aim to gather global datasets. Complementary efforts have also been made by Dawood et al. (2016) and Bahrampouri et al. (2021), who systematically compiled strong-motion archives in Japan.

In the case of Türkiye, the first recorded strong-motion data dates back to 1976. Over the subsequent years, the strong-motion network in Türkiye has progressively expanded, resulting in a substantial repository of accelerometric data accumulated over several decades. The initial comprehensive compilation of Türkiye's strong motion database was conducted by Akkar et al. (2010), encompassing 4,671 ground-motion records from 1976 to 2007. Post-2007, additional records stemming from moderate and large magnitude earthquakes (e.g., the 2010 M_w 6.1 Kovancılar, 2011 M_w 5.8 Simav, and 2011 M_w 7.1 Van earthquakes) were incorporated into the RESORCE database (Akkar et al., 2014). Furthermore, Alipour et al. (2020) compiled 1,189 ground-motion records captured at AFAD (Disaster and Emergency Management Authority) stations between 2008 and 2015, including pertinent site parameters.

Notably, in 2019, AFAD initiated the dissemination of the national strong-motion database (TADAS; tadas.afad.gov.tr; last accessed 15th March 2023), providing fundamental event information derived from fast moment tensor solutions published by the same institution. However, the waveforms contained in TADAS are generally processed with fixed filter cut-off frequencies and lack critical source and ground motion attributes such as tectonic regime, finite-rupture model, associated distance metrics, as well as flags indicating hanging-wall and pulse-like records. The absence of these essential metadata elements restricts the utility of TADAS for hazard and engineering studies, thereby motivating the need to update Türkiye's strong-motion database.

1.2 Scope of the Thesis

The primary objective of this thesis is to compile all available strong-motion events available in AFAD repository between 1976 and 2023 with up-to-date engineering parameters that are applicable to studies on engineering seismology and earthquake engineering. The secondary objective is to create an automatic algorithm for ground-motion processing. With the expansion of Turkish Strong-Motion Network, number of records per year can't be processed with manual processing methods. The February 6th, 2023 earthquake series (Pazarcık and Elbistan earthquakes, and their aftershocks) are good example, nearly 13,000 three-component waveforms are recorded in a month.
2

Especially, the need for rapid dissemination of recordings such an algorithm is mandatory.

1.3 Contributions

In this research, a new updated Strong-motion Database of Türkiye was compiled with a methodology that can be applied in future updates.

- All usable records from AFAD were processed.
- Necessary metrics for engineering usage are provided.
- An automatic processing algorithm to increase the number of available processed records was developed.

1.4 Organization

Chapter 1 presents the literature review, the scope of the thesis and contributions to the literature.

Chapter 2 of the thesis gives details about the development of the database in 5 sections. The details regarding the development include the calculation and compilation of the aforementioned engineering earthquake parameters, and overall rules set for the future updates.

Chapter 3 primary focus is the processing schemes, both manual and automatic methods. For manual methods, methodology utilized by the previous region-specific projects, such as T-NSMP, are directly used. Rules about the applicability of schemes are determined. For the automatic processing scheme, a general overlay of different studies that are applied are highlighted. Details for a preprocessing algorithm developed for this thesis is also included, and the efficiency of the automatic processing algorithm was tested with manual results. Finally, a new magnitude dependent flow-cut equation has been proposed for quick processing of records.

Chapter 4 gives the database in metadata form, to give a summary of the flatfile created under the scope of the thesis. These values include number of available records, availability of site-specific parameters, usable period ranges, available record in different earthquake types and style of fault and distance metric distribution for different magnitude events.

Chapter 5 is the conclusion part of the thesis. A summary of the thesis is provided with the conclusions about strong-motion databases, and the current situation of SMD-TR are explained in this chapter. Finally, possible updates for SMD-TR to increase its reliability by either improving the current methods or providing additional information for the events are outlined.

2. THE DATABASE DEVELOPMENT

The Strong-Motion Database of Türkiye (SMD-TR) is a comprehensive repository comprising 95,890 waveform data derived from 9,244 distinct seismic events provided by AFAD, recorded across 1,022 stations. This dataset is systematically categorized into five principal components: (1) event Information, (2) station Information, (3) source-to-site distance metrics, (4) Waveform Information, and (5) Intensity Measures (ground acceleration, velocity, and displacement), duration of strong-motion events, and parameters related to spectral analysis. The ensuing sections expand upon the methodologies underpinning the compilation of information within each of these

2.1. Event Information

Earthquake characteristics encompass a range of essential parameters, including a unique event identifier, the time of origin, the geographical coordinates of the hypocenter (latitude and longitude), as well as the focal depth at which the seismic event occurred. Furthermore, it encompasses the earthquake magnitude assessed through diverse scales such as moment magnitude (M_w), local magnitude (M_L), and duration magnitude (M_d). Additionally, details about the style of faulting, solutions regarding the moment tensor solution, fault dimensions, depth-to-the-top-of rupture (referred to as Z_{tor}), the tectonic regime (whether it is crustal or subduction), and indicators denoting events as aftershock or mainshock.

The compilation of event-related data is accomplished through sources that include literature survey research and seismological organizations. In this regard, the Disaster and Emergency Management Authority of Turkey (AFAD) holds the utmost priority for providing information regarding the origin time of earthquakes and the use of magnitude scales other than moment magnitude. For other earthquake parameters, such as epicentral coordinates, focal depth, moment magnitude, and moment tensor solutions, information is sourced from a combination of scientific literature and both local and global seismological agencies. A detailed breakdown of data sources and their respective importance in compiling event-related information is presented in Table 2.1.

5

Table 2.1. Hierarchy (ranking) applied to different data sources in the compilation of event information. The numbers inside the parenthesis indicate the total number of events, which used the specific event information from the designated data source. The full names of seismological agencies are given at the bottom of the table.

Hierarchy	Hypocenter Location	M_w	Moment tensor solution
1	ISC-GEM (186)	Literature Survey (38)	Literature Survey (65)
2	ISC-EHB (359)	ISC-GEM (147)	ISC-GEM (47)
3	ISC-Reviewed (3586)	Akkar et al. (2010) (29)	Akkar et al. (2010) (29)
4	AFAD (5113)	ISC (0)	ISC (158)
5		GCMT (201)	GCMT (246)
6		USGS (93)	USGS (92)
7		NEIC (3)	NEIC (3)
8		GFZ (28)	GFZ (32)
9		MED_RCMT (203)	MED_RCMT (195)
10		KOERI (43)	KOERI (42)
11		ZUR_RMT (15)	ZUR_RMT (19)
12		AFAD (3216)	AFAD (565)
13		ATH (13)	ATH (12)
14		UOA (16)	UOA (15)
15		OCA (13)	OCA (12)
16		ATA (1)	ATA (1)
17		NIC (8)	NIC (0)
18		AUTH (2)	AUTH (2)

AFAD: Disaster and Emergency Management Presidency; ATA: The Earthquake Research Center Ataturk University; ATH: National Observatory of Athens; AUTH: Aristotle University of Thessaloniki; GCMT: The Global CMT Project; GFZ: Helmholtz Centre Potsdam GFZ German Research Centre For Geosciences; ISC: International Seismological Centre; ISC-EHB: Engdahl, van der Hilst, and Buland global data set; ISC-GEM: ISC Global Instrumental Earthquake Catalogue; ISC-Reviewed: The Reviewed ISC Bullettin; KOERI: Kandilli Observatory and Earthquake Research Institute; MED_RCMT: MedNet Regional Centroid - Moment Tensors; NEIC: National Earthquake Information Center; NIC: Cyprus Geological Survey Department; NOA: National Observatory of Athens; OCA: Observatoire de la Côte d'Azur; UOA: University of Athens; USGS: U.S. Geological Survey; ZUR_RMT: Zurich Moment Tensors.

The initial step in establishing event parameters involves determining the geographic location of earthquakes, specifically their latitude, longitude, and focal depth. This geographic data, when available, is sourced from various databases, which are the International Seismological Centre's Global Earthquake Model (ISC-GEM), ISC-EHB, and ISC-Reviewed-Bulletin (International Seismological Centre, 2023; Bondár and Storchak, 2011; Di Giacomo et al., 2018; Lentas, 2019; Storchak et al., 2020; Engdahl et al., 2020). If any of these ISC databases lacks location information for a given event, geographical data provided by the Disaster and Emergency Management Authority of Turkey (AFAD) was accepted as final.

Approximately 6% of the entire dataset of 9,244 events draws location information from ISC-GEM and ISC-EHB. ISC-Reviewed-Bulletin and AFAD contribute 39% and 55%, respectively, to the geographical data within the SMD-TR. It's noteworthy that the location data in ISC-Reviewed-Bulletin is regularly updated, with the current version extending up to 2021. Consequently, revision of the event location information, along with any pertinent seismic parameters, based on the latest ISC-Reviewed-Bulletin will occur as the bulletin gets updated.

The second phase in establishing event parameters involves the acquisition of Moment Magnitude (M_w) data, and consequently, moment tensor solutions, from seismological agencies. The sources of this data, their ranking, and the number of events utilizing each data source for M_w are provided in Table 2.1. In compilation of the event parameters, event information from previous database projects such as TNSMP (Akkar et al., 2010), SHARE (Yenier et al., 2010), RESORCE (Akkar et al., 2014), EMME (Danciu et al., 2018), and TSTHG (Akkar et al., 2018) were also considered.

The third and final step in compiling event parameters involves integrating information garnered from event-specific studies. A similar approach to RESORCE was followed in incorporating additional studies as well. To achieve this, the ISC search tool (Di Giacomo et al., 2014) was employed for moderate to large magnitude events ($M_w \geq 5.5$) in the database. Articles containing moment tensor solutions, either regarding geometry or dimensions, for small-magnitude events ($M_w < 5.5$), are also included. Additionally, moment tensor solutions published by local institutions such as KOERI reports (http://www.koeri.boun.edu.tr/sismo/2/en/) was searched. The electronic supplement to this article includes a list of 65 earthquakes for which parameters were obtained from literature sources.

All events encompass complete epicentral location and origin time information. Focal depth data, however, is unavailable for 41 events. Out of the 9,244 events, 44% have reported M_w values. Unlike TNSMP and RESORCE, no magnitude conversion equations are applied to standardize magnitudes in SMD-TR. Nevertheless, the use of established, peer-reviewed empirical magnitude conversion equations, such as those detailed in Akkar

et al. (2010) are recommended if such standardization is required. Among the events, 43% have local magnitude (M_L) values, while 13% are characterized by duration magnitude (M_d). Notably, all events with $M_w > 6.1$ are accompanied by moment tensor solutions. With the exception of eight events out of a total of 129, earthquakes with $M_w \geq 5.5$ have comprehensive fault geometry information compiled from either literature sources or seismic agencies.

The classification of the style-of-faulting (SoF) is ascertained through the application of criteria introduced by Boore and Atkinson (2007), as outlined in Table 2.2. This methodology aligns with the approach adopted in RESORCE flatfile. The determination relies on the plunge angles associated with the T- and P-axes derived from double-couple fault-plane solutions. These solutions are acquired from either the seismic agencies specified in Table 2.1 or from literature references provided in the electronic supplement.

Table 2.2. Style-of-faulting definitions by Boore and Atkinson (2007)

Style of faulting	P-axis plunge angle	T-axis plunge angle
Normal	P-pl>40°	T-pl<40°
Reverse	P-pl<40°	T-pl>40°
Strike-slip	P-pl<40°	T-pl<40°

The classification of earthquakes follows the methodology delineated in Garcia et al. (2012). This classification framework is grounded in the tectonic environments and stratifies events into various subtypes. For crustal events, these subtypes encompass shallow and deep active crustal, with a focal depth of 35 km serving as the boundary between the two. Additionally, the classification encompasses subduction events, SZ interface and SZ inslab, as well as stable continental events, as depicted in Figure 2.1. Notably, while modeling the Hellenic and Cyprus arcs, the "Slab2 Model" devised by Hayes et al. (2018) was employed. This model offers the advantage of encompassing the geometric attributes of the slab along the southwestern coast of Türkiye towards Greece while furnishing a comprehensive slab model for the Hellenic and Cyprus arcs.

The classification process is executed exclusively for earthquakes with available moment tensor solutions. In total, 1,536 earthquakes with fault plane solutions have been successfully classified, and a detailed breakdown for each earthquake class is provided in Table 2.3. However, it is important to note that a subset of earthquakes remains unclassified, primarily due to the absence of moment tensor solutions in their respective datasets.

Table 2.3. Number of events for each earthquake class

Class	Number of events
Shallow active crustal	1452
Deep crustal	8
Subduction Interface	12
Subduction Intra-slab	63
Outer trench	1

Additionally, a declustering analysis employing the windowing algorithm as introduced by Gardner and Knopoff (1974) was conducted. For this purpose, the ZMAP algorithm developed by Wiemer (2001) was utilized, which considers earthquake magnitude, geographical coordinates, and the temporal occurrence of earthquakes to identify aftershocks within the dataset. This analysis revealed a total of 5,165 dependent earthquakes out of the initial dataset of 9,244.
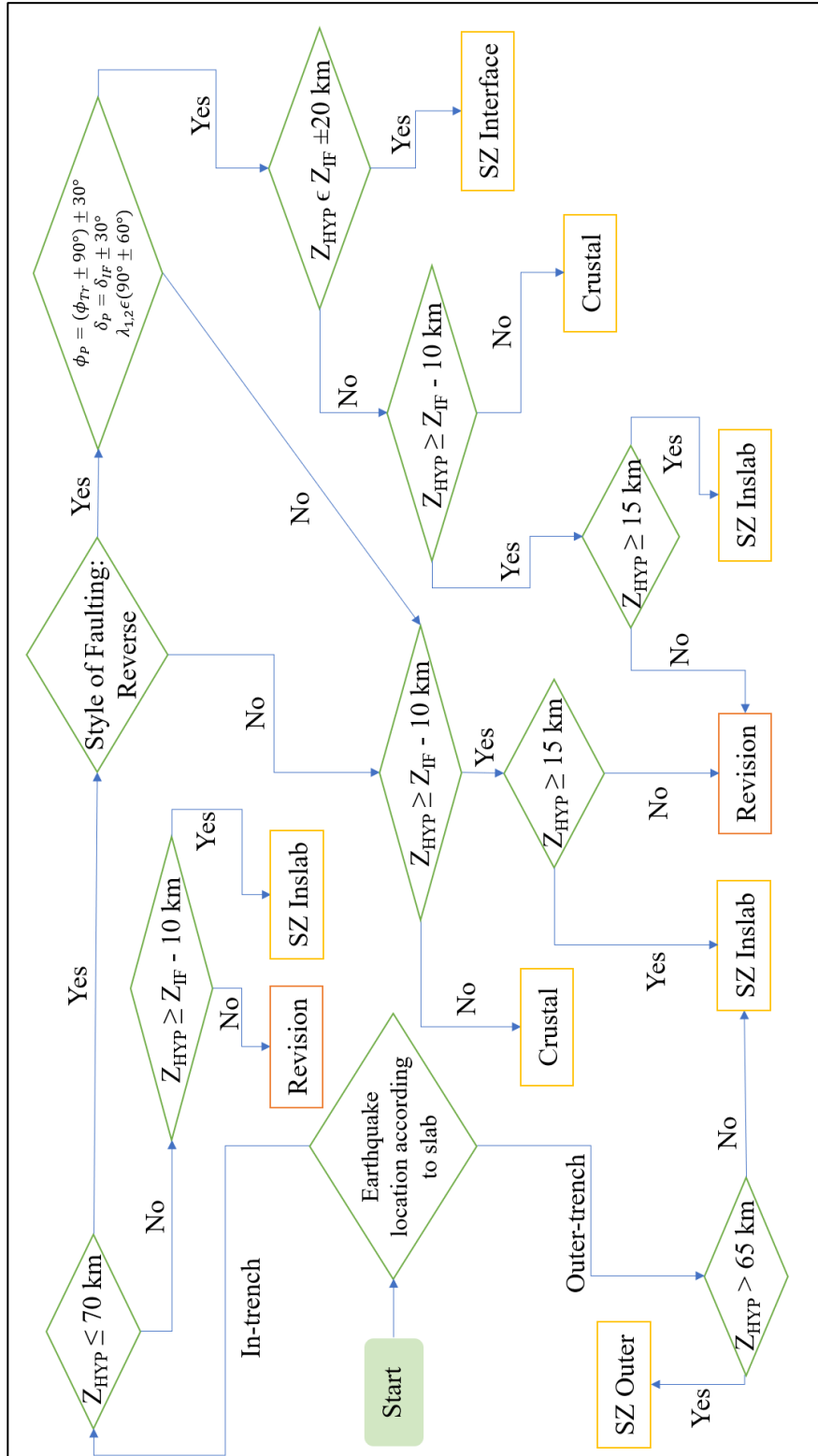
Figure 2.1. Earthquake classification by Garcia et al. (2012). The acronyms are: Z_{HYP}: focal depth; Z_{IF}: interface depth at the epicenter; φ_P: P-axis strike; φ_{Tr}: trench strike; δ_P: P-axis plunge; δ_{IF}: interface dip at the epicenter; $\lambda_{1,2}$: rake angles of the two nodal planes; Shallow Crustal: $Z_{HYP} < 35$ km; Deep Crustal: $Z_{HYP} > 35$ km).

2.2. Station Information

The station parameters, sourced from AFAD, encompass essential details including network names and codes, location specifics such as station latitude, longitude, and elevation. This information is complemented by station address data and sensor-related particulars, including sensor installation date (and removal date if inactive), sensor type, and associated properties such as sensor serial number, recorder serial number, frequency, gain settings, and calibration parameters.

Of particular importance among the site parameters are the time-based average values of shear wave velocity in the uppermost 30 meters (V_{S30}) and the depth-to-the-rock layer (referred to as Z1, denoting the depth at which V_S reaches a horizon of 1.0 km/s). Among the 1,022 stations in the dataset, 679 stations have provided measured VS profiles. These profiles have been obtained through in-situ geophysical techniques, including the multi-channel analysis of surface waves (MASW) and passive Remi field tests, conducted as part of the TUBİTAK and UDAP projects (Sandıkkaya et al., 2010; Kurtuluş et al., 2018). It is noteworthy that AFAD periodically conducts site characterization campaigns for active sensors in the field, and as these new data sets become available, they will be incorporated into future versions of the SMD-TR dataset.

2.3. Source-to-Site Distance Metrics

A comprehensive set of distance metrics for both point-source and finite-source scenarios was compiled, in addition to indicating the hanging wall status and pulse period for each recorded event. SMD-TR incorporates the epicentral distance (R_{epi}) for all records, and when the focal depth is available, the hypocentral distance (R_{hyp}) is also provided, with the exception of 67 records where this information is missing.

For events in which the "true fault geometry" is ascertainable (valid for 8,500 records), the methodology outlined by Akkar et al. (2014) to calculate finite-fault distance metrics was employed. These metrics encompass the closest distance to the surface projection of the fault rupture plane (R_{JB}, Joyner-Boore distance) and the nearest distance to the fault rupture plane itself (R_{rup}). Furthermore, hanging wall/footwall flags were provided in the

11

database, along with R_X and R_Y values. As described by Ancheta et al. (2014), R_X is defined as the distance perpendicular to the fault strike from the surface projection of the up-dip edge of the fault plane, while R_Y measures the distance parallel to the fault strike from the midpoint of the surface projection of the fault plane.

It's noteworthy that seismic intensity measures recorded on stations situated on the hanging wall side of the rupture typically exhibit higher values than those on the footwall side. To identify these stations, a hanging wall flag in the database was incorporated, following the approach delineated by Donahue and Abrahamson (2014). This approach considers that the hanging wall effect is most pronounced in the area perpendicular to the fault length, diminishing as both the absolute values of R_Y and R_X increase, ultimately dissipating at the ends of the rupture (Donahue and Abrahamson, 2014; Figure 7).

For events where the "true fault geometry" remains unknown, despite having fault plane solutions (applicable to 28,326 records), mean R_{JB} and R_{rup} values were calculated using information from both fault planes provided by the fault plane solutions. In such cases, R_X and R_Y distance metrics are not provided, and hanging wall flags are included only if both fault planes yield consistent information. If fault plane solutions are unavailable or yielding conflicting results, they are flagged as "unavailable" or "undecided" respectively.

Identification of pulse-like records and determination of their pulse periods are accomplished using the algorithm detailed in Shahi and Baker (2014). This algorithm relies on wavelet transform techniques to detect pulse signals and extract pulse-related features. Subsequently, energy and peak velocity ratios are employed to compute the pulse indicator. Records with negative pulse indicators are categorized as non-pulse-like, while those with positive indicators are deemed pulse-like.

2.4. Waveform Metadata

Essential waveform metadata, encompassing details regarding waveform quality, processing methodology, the cut-off values for low- and high-pass filters, and the usable periods for each record were included in the dataset.

For records that underwent manual processing in prior studies (1,162 records from Akkar et al., 2014, and 1,383 records from Alipour et al., 2020), their reliability is acknowledged, and the low- and high-cut filter frequency values from these studies are directly adopted for this study. Subsequently, an additional 3,092 records designated as having "engineering significance" (associated with events featuring $M_w > 5.5$) were subjected to manual processing in the present study.

The remaining waveform data, totaling 90,253 records, were processed using an automatic processing algorithm. Within this subset, 40,431 records were classified as having poor quality. Details for the number of components processed by the two schemes are detailed in Table 2.4.

In the subsequent section, comprehensive details regarding the waveform data processing procedures will be provided. In the final phase, the usable periods for the processed records were calculated by a method outlined in Akkar and Bommer (2006) and Ancheta et al. (2014).

Table 2.4. Number of processed records by filtering schemes

Number of Components Processed	Manual Processing	Automatic Processing
3	5545	33223
2	6	9598
1	2	7001
0	84	40431
Total	5637	90253

2.5. Intensity Measures

The SMD-TR dataset offers a comprehensive set of ground-motion parameters derived from the processed accelerometric data. These parameters encompass peak ground acceleration (PGA), peak ground velocity (PGV), peak ground displacement (PGD), Cumulative Absolute Velocity (CAV), Arias Intensity (AI), and significant duration values for 5-95%, 5-75% and 20-80%. Additionally, pseudo-spectral accelerations (PSA) at 5% damping are provided for 111 periods, ranging from T = 0.01 seconds to T = 20 seconds, for each component of the recorded data.

Furthermore, the dataset includes orientation-independent horizontal spectra, specifically the RotD50 and RotD100 values. These values correspond to the 50th and 100th percentiles of the distribution of the rotated intensity measures. The calculations for these spectra are performed using the RCTC code, as outlined in Wang et al. (2017).

3. RECORD PROCESSING SCHEMES

The primary objective of waveform filtering is to eliminate both high and low-frequency noise from the waveforms while preserving the fundamental characteristics of the earthquake signal. Prior studies, including Akkar et al. (2010), Akkar et al. (2014), Alipour et al. (2020), and Kale et al. (2023), have already processed certain waveforms present in the SMD-TR dataset. In order to ensure consistency and continuity across these projects, the filter cut-off values they established were opted to be used in this study.

Given the substantial number of new records incorporated into the SMD-TR dataset, a combination of manual and automatic processing approaches for waveform processing were employed. The most notable distinction between these two methods lies in the determination of low and high-cut filter frequency values (referred to as f_{lc} and f_{hc}, respectively) used to filter out noise from the waveforms.

In the manual processing approach, expert judgment is the primary factor in determining f_{lc} and f_{hc} to effectively remove noise from the waveforms. On the other hand, the automatic processing scheme employs an algorithm to autonomously calculate f_{lc} and f_{hc}, albeit with certain limitations.

In this study, the manual processing scheme was applied to the waveforms deemed to be of engineering significance ($M_w \geq 5.5$). For the remainder of the database, the automatic processing scheme was utilized. This dual approach allows us to efficiently process a large volume of data while ensuring that critical records are subjected to expert-guided filtering to maintain data quality and reliability.

3.1. Manual Processing Scheme

The manual processing scheme employed for SMD-TR closely adheres to the procedure outlined by Akkar et al. (2014). This scheme involves several key steps:

- **Visual Screening**: The initial step involves a visual inspection of the three-component waveforms to identify and exclude records with non-standard errors, as described in Douglas (2003). Out of the total 5,637 records, only 84 records (comprising 252 components) were excluded due to poor waveform quality.

- **Zero-Order Correction**: Following visual screening, a zero-order correction is applied. This correction involves removing the mean acceleration value from the entire waveform.

- **Determination of f_{lc} and f_{hc} Values**: The next step is the determination of low-cut (f_{lc}) and high-cut (f_{hc}) filter frequency values. These values are determined using procedures proposed by Boore and Bommer (2005) and Douglas and Boore (2011).

- **Band-Pass Filtering**: An acausal 4-pole Butterworth band-pass filter is applied to 5,553 records to isolate the desired frequency range of interest which effectively removes noise from the waveforms.

- **Post-Processing**: Lastly, a post-processing procedure detailed in Boore et al. (2012) is employed to remove zero pads introduced during the band-pass filtering process.

For more in-depth information regarding the manual processing scheme, readers can refer to the following studies: Boore and Akkar (2003), Boore and Bommer (2005), Akkar et al. (2010, 2011, 2014), Douglas and Boore (2011), and Boore et al. (2012). These articles provide comprehensive details and visual aspects of the manual record processing procedure for those interested in a deeper understanding.

3.2. Automatic Processing Scheme

In the processing of the SMD-TR dataset, two automatic processing algorithms were explored to determine the low-cut (f_{lc}) and high-cut (f_{hc}) filter frequency values. These algorithms are as follows:

Dawood et al. (2016) Algorithm: This algorithm, applied to the Japanese KiK-Net database, is characterized by its speed and relatively short processing time. However, it tends to produce conservative f_{lc} values, occasionally exceeding the actual low-frequency content of the record (f_a).

Rennolet et al. (2018) Algorithm (APS): This alternative, utilized for processing earthquake waveforms recorded in Oklahoma and Kansas in the United States, was chosen due to its ability to provide more accurate f_{lc} and f_{hc} values. The APS comprises preprocessing, f_{lc} and f_{hc} determination, band-pass filtering, and post-processing steps.

To ensure the robustness of the automatic processing, an algorithm was designed to detect nonstandard errors or digitization problems present in the unprocessed waveforms. Detecting and addressing such errors are critical, as they can affect the proper determination of f_{lc} and f_{hc} values by the APS.

The classification of waveforms is conducted based on their quality, resulting in three categories:

Good-Quality Waveforms: These waveforms do not exhibit nonstandard errors or digitization problems.

Low-Quality Waveforms: This category includes waveforms that may contain issues such as moderate insufficient digitizer resolution (IDR), early termination during the coda (ETDC), or multiple shocks (MS). They can be processed after specific treatments, such as removing spikes, or determination of the time window for the mainshock.

Bad-Quality Waveforms: This category encompasses waveforms with severe issues, including S-wave triggered (S-WT), poor or very poor IDR, miscellaneous errors like baseline shifts, high noise, or random spikes, etc. These waveforms are excluded from processing (labeled as BQ in the dataset).

The APS algorithm determines f_{lc} and f_{hc} values by evaluating the signal-to-noise ratio (SNR), which involves comparing the Fourier amplitude of the signal to that of the noise. The Fourier amplitude spectra of noise are computed from the pre-event portion of the accelerometric data. The discrete frequency values at which SNR exceeds 2 for the first

and last time are defined as f_{lc} and f_{hc}, respectively. After selecting these values, the waveforms undergo bandpass filtering and the same post-processing steps as outlined in the manual processing scheme are applied.

This comprehensive approach aims to enhance the accuracy and reliability of the processed waveforms while accounting for various data quality scenarios.

Initial assessment of the Automatic Processing Scheme (APS) began with an examination of manually processed records falling within the magnitude range of $5 \leq M_w \leq 6$. This was particularly relevant as a subset of records with relatively low magnitudes was manually processed. The objective was to ensure the appropriateness of the low-cut filter cut-off values determined by APS.

The left panel of Figure 3.1 illustrates the ratio statistics of f_{lc} values determined by the automatic and manual processing schemes. Ratios close to 1 indicate a good agreement between the two processing methods. The histogram in this panel reveals that a significant portion of the ratios (58% of the entire dataset) falls within the range of 1 ± 0.10, indicating a high degree of consistency between the two methods.
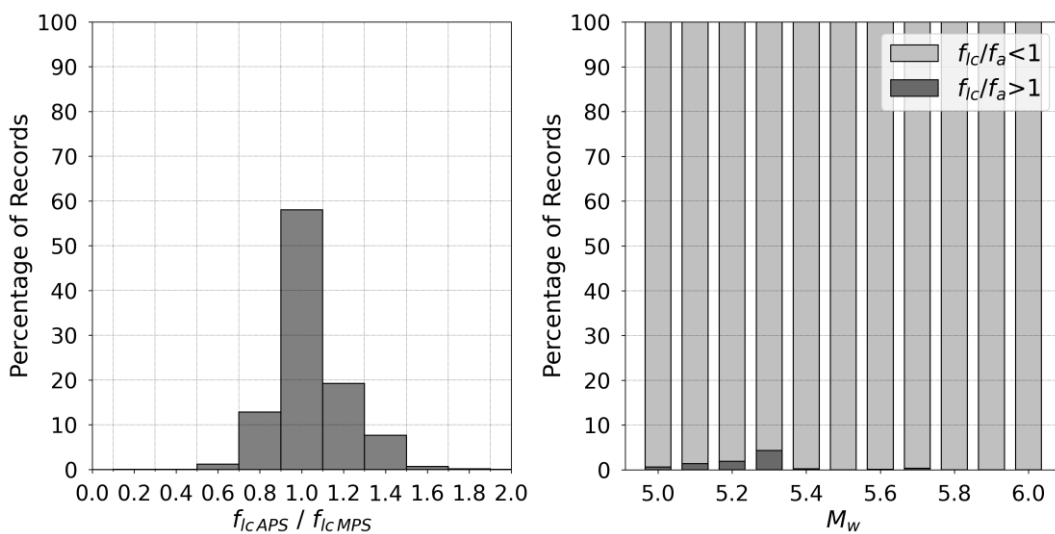
Figure 3.1. Comparison of f_{lc} determined from manual processing scheme (MPS) and APS, and magnitude dependency of f_{lc} by APS.

The right panel in Figure 3.1 depicts the ratio statistics of f_{lc} determined by APS, normalized with the magnitude-dependent variation of fa. A ratio greater than 1 would imply that APS's low-cut filter cut-offs are likely to distort the actual ground-motion frequencies at the low-frequency end. The magnitude-dependent ratio statistics suggest some distortion of low-frequency ground-motion components by APS, particularly for events with $M_w \leq 5.3$. However, even for the M_w 5.3 case (where the most significant distortion was observed), the probability of low-frequency distortion by APS does not exceed 4.3%.

A secondary study for the efficiency of APS in high magnitude earthquakes was tested by using the records of the February 6th, 2023 Pazarcık and Elbistan earthquakes. All of the visually inspected and manually processed records were compared by low cut filter frequency values.

Figure 3.2 shows the comparison of f_{lc} values chosen by MPS and APS. While APS provides conservative values for moderate magnitudes ($5 \leq M_w \leq 6$), for Pazarcık and Elbistan earthquakes, it computes lower f_{lc} values than MPS. This also highlights that a large magnitude earthquake should be processed by visual inspection and manual filter cut-off selection.
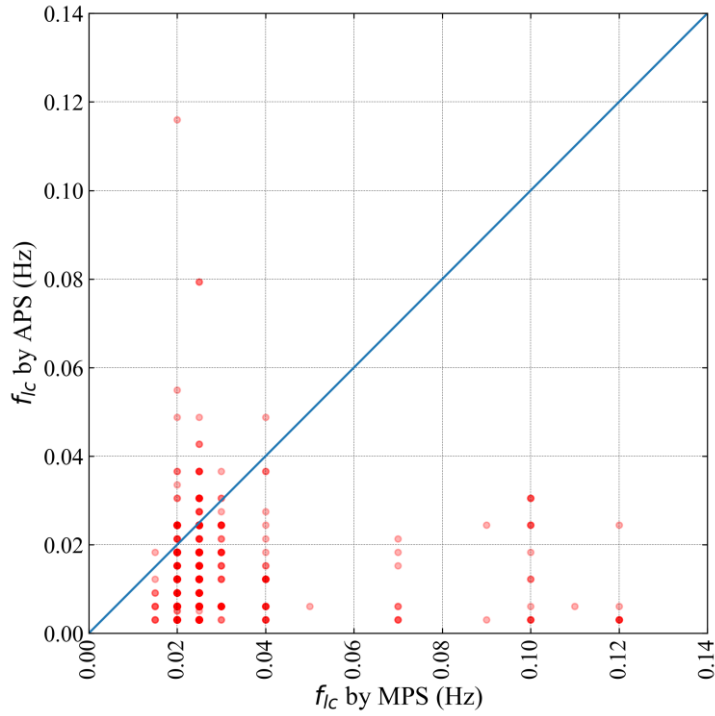
Figure 3.2. Comparison of f_{lc} values by APS and MPS for Elbistan and Pazarcık earthquakes.

Based on these observations, it was concluded that the use of the automatic processing scheme is both feasible and acceptable for processing waveforms within the specified magnitude range. The results indicate that while some distortion occurs for lower magnitude events, it remains within reasonable limits and is unlikely to significantly impact the analysis of ground-motion data.

Table 3.1 presents an overview of the number of processed records in the database. Out of the total 90,253 three-component recordings that underwent automatic processing, a substantial number of components (144,893) were flagged as bad-quality and subsequently excluded from processing. These bad-quality records were identified due to various reasons, including the presence of nonstandard errors, signal-to-noise ratios less than two, or recordings with low-cut filter frequency value (f_{lc}) exceeding 1 Hz or high-cut filter frequency value (f_{hc}) less than 10 Hz.

Table 3.1. Number of processed records by APS in component-wise

Components	Number of Records
3-component	33,223
Only two horizontal components	6,403
One horizontal and vertical components	3,195
Only one horizontal component	5,379
Only vertical component	1,622

The remaining 125,866 components, deemed to be of sufficient quality, proceeded through the band-pass filtering and post-processing steps as part of the automatic processing scheme.

The left panel of Figure 3.3 illustrates the magnitude-dependent variation of f_{lc} values for both manually processed and automatically processed waveforms. In addition, this plot includes the variation of f_a in the theoretical source spectrum as proposed by Atkinson and Silva (2000) for reference. The selected f_{lc} values are generally lower than f_a, with only 1% of the waveforms having f_{lc} values exceeding their respective f_a values. This statistic indicates that APA for record processing, in nearly all cases, does not remove the actual frequency content of the records. The color-coded circles in the figure represent groups of records processed with specific f_{lc} values, with darker colors (ranging from yellow to red) indicating larger numbers of records in the respective f_{lc} group.

From this plot, a strong correlation between f_{lc} and earthquake magnitude (M_w) is evident (i.e., the seismic moment corner frequency relation proposed by Brune 1970), paralleling the trend line of f_a vs. M_w in blue. As magnitude increases, f_{lc} values tend to decrease. While not shown in this plot, it's worth noting that both event-specific and site-specific characteristics of the recording station (e.g., R_{JB}, V_{s30}) have substantial effects on f_{lc} values.

To separate the effects of M_w from those related to earthquake and site characteristics, a robust linear mixed-effects regression algorithm (Koller, 2016) was applied to establish a M_w-dependent f_{lc} relation (denoted as Eq. 1). This algorithm was preferred instead of least-square regression or random effects regression to achieve lower weights for outlier points in computation of model coefficients. This relation, which prefers a quadratic form but caps f_{lc} values for $M_w > 6$, is particularly valuable for making preliminary (rapid) decisions on f_{lc}, especially after significant events, such as the recent Kahramanmaraş earthquakes on February 6th, 2023. In this relation, the median relation $(\overline{f_{lc}})$ is provided, along with its $\pm\sigma$ estimates (σ=0.58 in ln units). The mean M_w-f_{lc} combinations considered in the NGA-West2 database are also plotted in the same panel for comparison.

Notably, the NGA-West2 f_{lc} values and estimations of this study from Eq. 1 closely align at small magnitudes. However, in the intermediate magnitude range, on average, the NGA-West2 database tends to use higher f_{lc} values than those suggested by Eq. 1. The difference between NGA-West2 and median f_{lc} values of this study (derived from Eq. 1) becomes negligible at larger magnitudes.

$$ln\overline{(f_{lc})} = 3.754 - 1.640\,min(M_w, 6) + 0.084\,min(M_w, 6)^2 \qquad (Eq.\ 1)$$
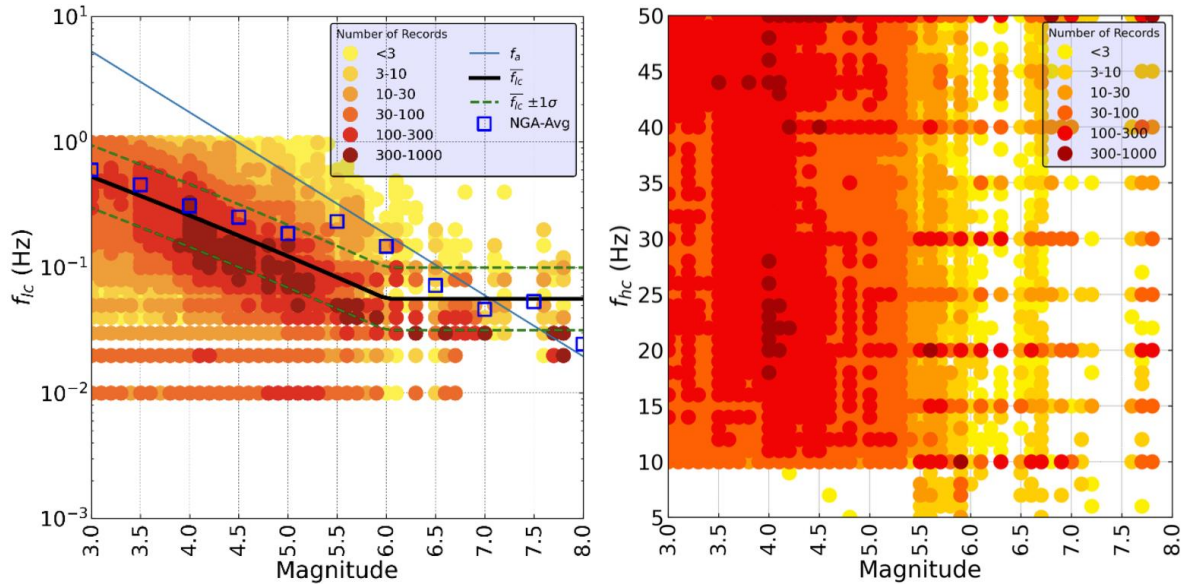
Figure 3.3. Magnitude dependency of (a) low-cut filter frequencies and (b) high cut filter frequencies

The right panel of Figure 3.3 provides similar information as the left panel but focuses on f_{hc} (high-cut filter cut-off) values. In this case, f_{hc} values generally cluster around 20 Hz, and no significant dependency on earthquake magnitude (M_w) is observed. Consequently, a constant f_{hc} value of approximately 20 Hz can be considered suitable for all waveforms during their preliminary (rapid) dissemination.

It's worth noting that f_{hc} has an insignificant effect on the short and very short period response spectral ordinates, as demonstrated by previous studies (Akkar et al., 2012; Douglas and Boore, 2011). To enable studies involving parameters like κ and Q, it's also viable to *use $f_{hc} = min$ (40 Hz, 0.8$f_{Nyquist}$)* for automatic processing.

Figure 3.4 presents the usable period range versus the number of records, considering the Akkar and Bommer (2006) usable spectral period criteria for manually processed waveforms and the 0.8/f_{lc} expression (as suggested in Ancheta et al., 2014) for automatically processed data. The criteria used to compute the usable period range do not exclude any of the processed data within the period interval of T = 0.01–0.8 seconds, encompassing approximately 45,000 records.
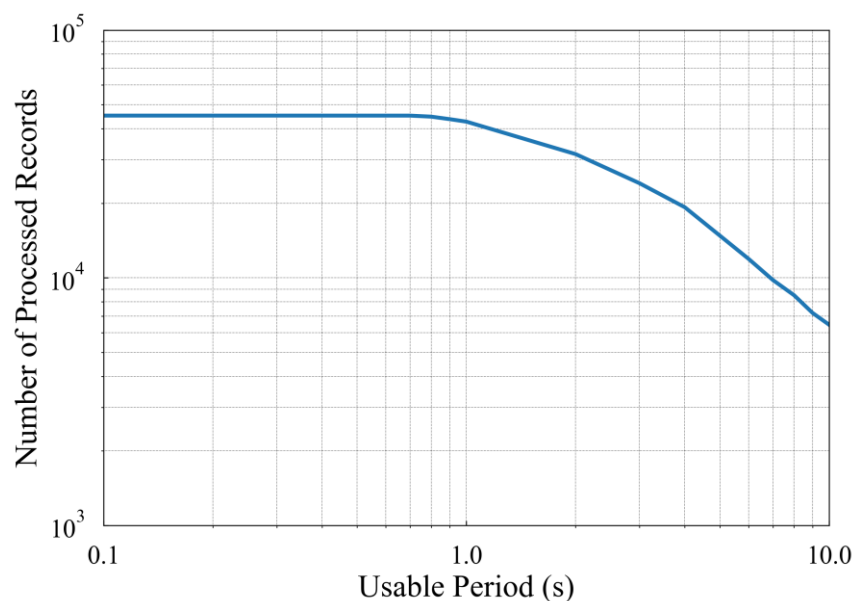
Figure 3.4 The usable period ranges of the horizontal-component ground motions in SMD-TR

The number of records begins to decline after T = 0.8 seconds, and this decrease becomes more pronounced after T = 4 seconds. As the oscillator period approaches T = 10 seconds, only 20% of the dataset remains, highlighting the diminishing availability of data for longer periods.

4. METADATA INFORMATION

The SMD-TR encompasses a total of 55,375 processed records originating from 6,710 events, which were recorded at 974 stations. It's important to note that the remaining 48 out of the 1,022 stations do not have any good-quality records. The processed records within SMD-TR provide seismological information, including details about the event (such as earthquake class, magnitude, fault type, and focal depth), site characteristics (V_{S30}, Z1), and source-to-site distance metrics.

Figure 4.1 presents a year-based variation of events (top row) and the corresponding processed ground motions (bottom row), specifically focusing on available magnitude information. The data accumulation exhibited notable growth after 1995, primarily attributed to an increase in instrument deployment within the national strong-motion network. It's worth noting that data accumulation, especially for smaller magnitude events, was relatively low between 1976 and 1994.

Parallel to the expansion in the number of stations from 1995 to 2010, there was a significant increase in strong-motion data accumulation. During this time span, the number of events recorded ranged from 21 to 187, with the maximum number of events (187) recorded in 1999, largely due to the earthquake sequences following the M_w 7.6 Kocaeli and M_w 7.2 Düzce events. The number of ground motions recorded within this period varied between 24 and 315. Scatter diagrams in Figure 4.1 also suggest that the lowest magnitude reliably captured by the strong-motion network during this time was M3.0.
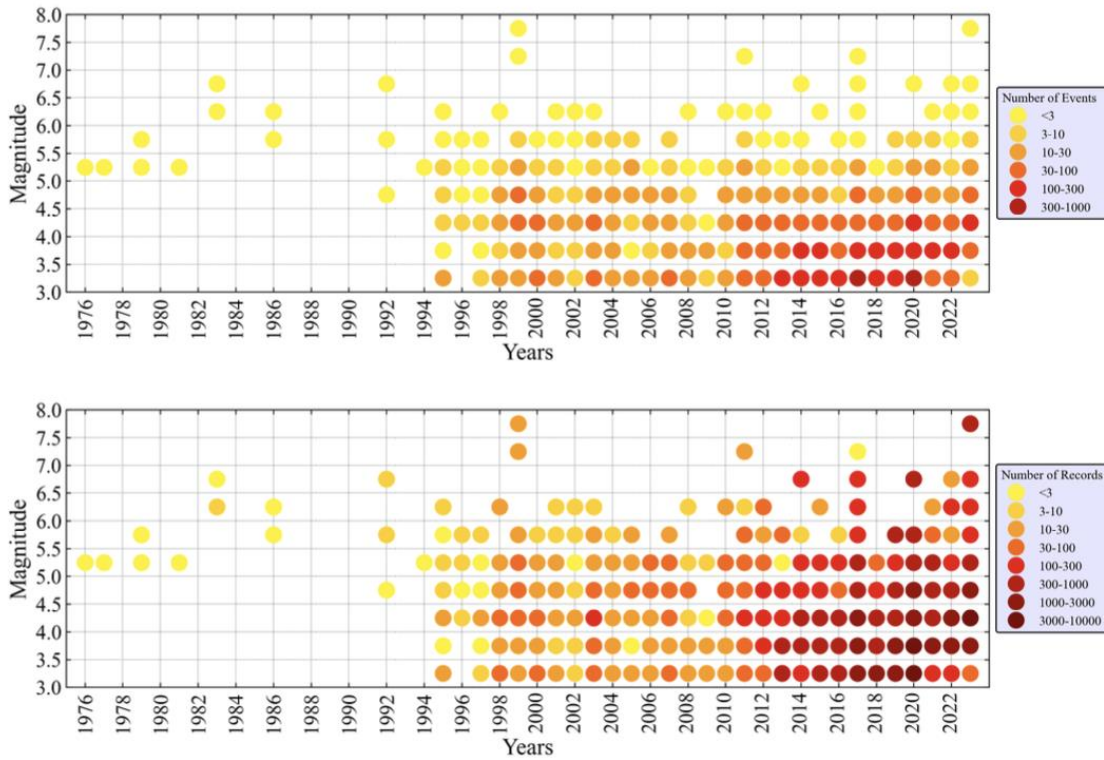
Figure 4.1. Yearly-based distribution of event numbers (top row) and records (bottom row) in terms of magnitude.

Starting in 2011, there was a substantial yearly increase in record numbers. For instance, in 2011, the database contained 279 events (including events from the M_w 5.8 Simav and M_w 7.1 Van earthquakes) and 632 processed records. By 2020, these numbers had grown to 1,039 events and 12,800 processed records, with significant data accumulation occurring following earthquake sequences like the M_w 7.0 Samos and Mw 6.8 Elazığ events. In 2023, the database contains approximately 13,000 recorded accelerometric data points within just one month following the February 6th, 2023, M_w 7.8 and M_w 7.7 Kahramanmaraş earthquakes. This highlights the database's ability to rapidly capture and store data from significant seismic events.

Figure 4.2 provides an overview of the progression in the availability of processed records for Türkiye. It's worth noting that the NGA-West2 database contains limited data from Türkiye, as it primarily focuses on global data with larger magnitudes. The previous database for Türkiye, known as T-NSMP and developed by Akkar et al. (2010), had limitations due to the sparse distribution of stations within the country.

However, there has been a significant increase in earthquake activity in Türkiye over the last decade, which has contributed to the growth of the SMD-TR database, especially for events with magnitudes greater than 6.5 and their associated aftershocks, even in smaller magnitudes. This expansion in available data is vital for enhancing earthquake research and seismic hazard assessment in Türkiye.
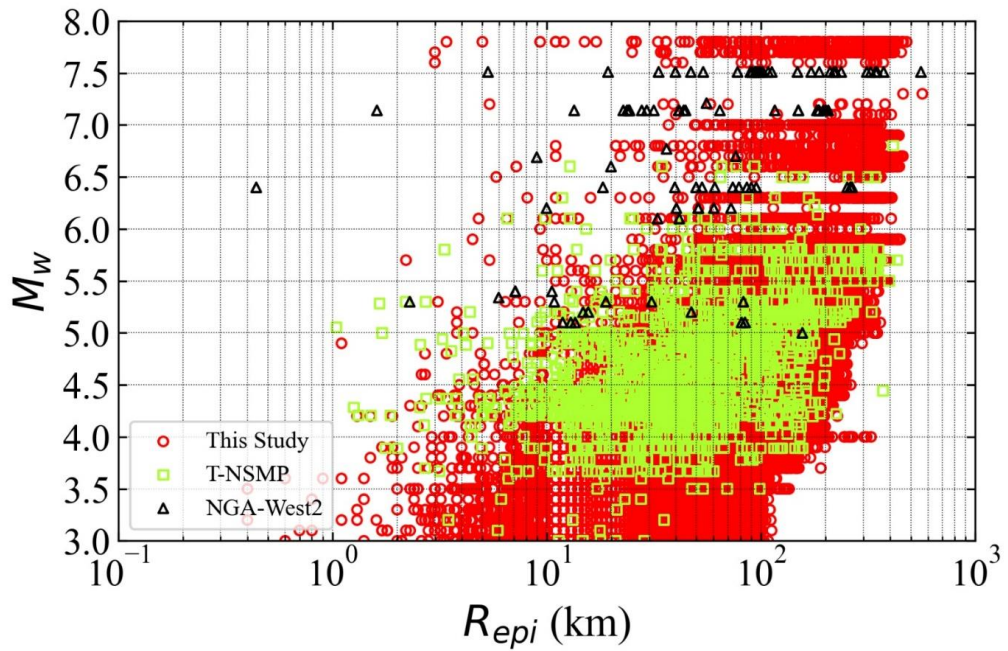
Figure 4.2. Processed available records from NGA-West2 and T-NSMP databases. Each database marker excludes the previous studies records.

The yearly-based average number of records per event (NRPE) is another important metric in earthquake monitoring. In the early years of the national network (1976-1994), NRPE ranged from 1 to 4 records per event, indicating limited data availability and coverage. However, with the dense instrument deployment that started in 1995 and continued in subsequent years, NRPE has shown a continuous increase.

In more recent years, the national network has been able to capture approximately 180 waveforms from moderate-to-large magnitude events ($M_w > 5.5$). This substantial increase in the number of records per event reflects the improved capacity of the network to capture and store a larger volume of data, which is crucial for seismic research, hazard assessment, and earthquake engineering in Türkiye.

Figures 4.3 to 4.6 provide a comprehensive geographic distribution of earthquakes in terms of magnitude, focal depth, style-of-faulting (SoF), and earthquake class. These figures are accompanied by an active tectonic map of Türkiye for context (Emre et al., 2013; Demircioğlu et al., 2018).

Figure 4.3 displays the spatial distribution of shallow crustal earthquakes based on magnitude. Yellow circles represent events with $M_w < 6$, while red diamonds represent events with $M_w \geq 6$. Different symbol sizes indicate various magnitudes.

Figure 4.4 focuses on the distribution of shallow crustal events, considering their SoF. Triangle, square, and star symbols represent reverse, normal, and strike-slip events, respectively. Deep crustal events (focal depths greater than 35 km) are also depicted in red, with the same symbols used for different SoF's. Figure 4.5 specifically illustrates the distribution of subduction earthquakes along the Mediterranean coast of Türkiye.

Figure 4.6 highlights events with unknown SoF or M_w information, and events in the southwestern part of Türkiye with focal depths deeper than 35 km are shown in red. These events are potentially subduction events but have been left unclassified due to the absence of moment tensor solutions.
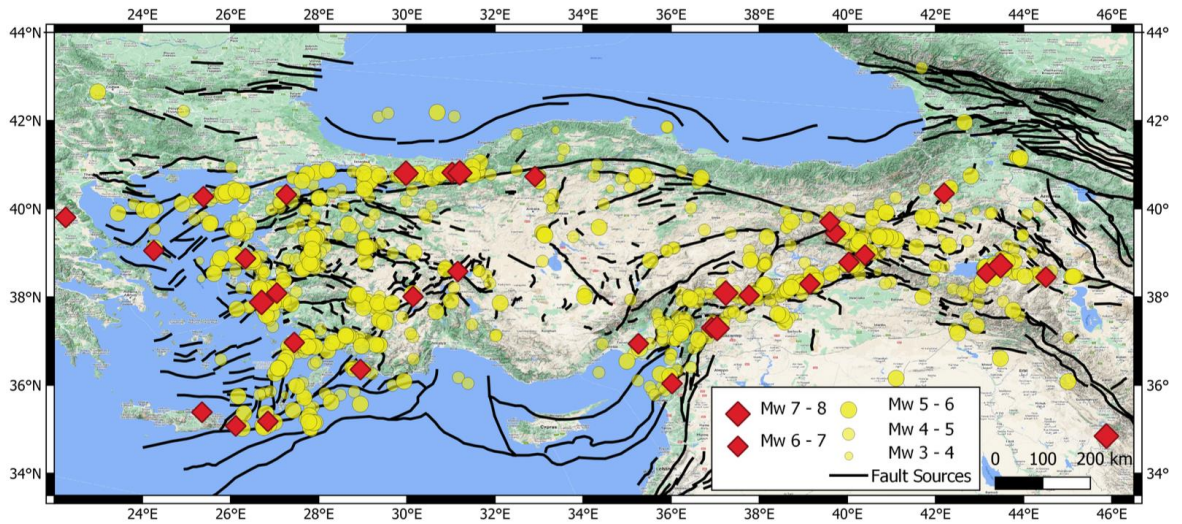
Figure 4.3. Geograpic distribution of shallow crustal events in terms of M_w.
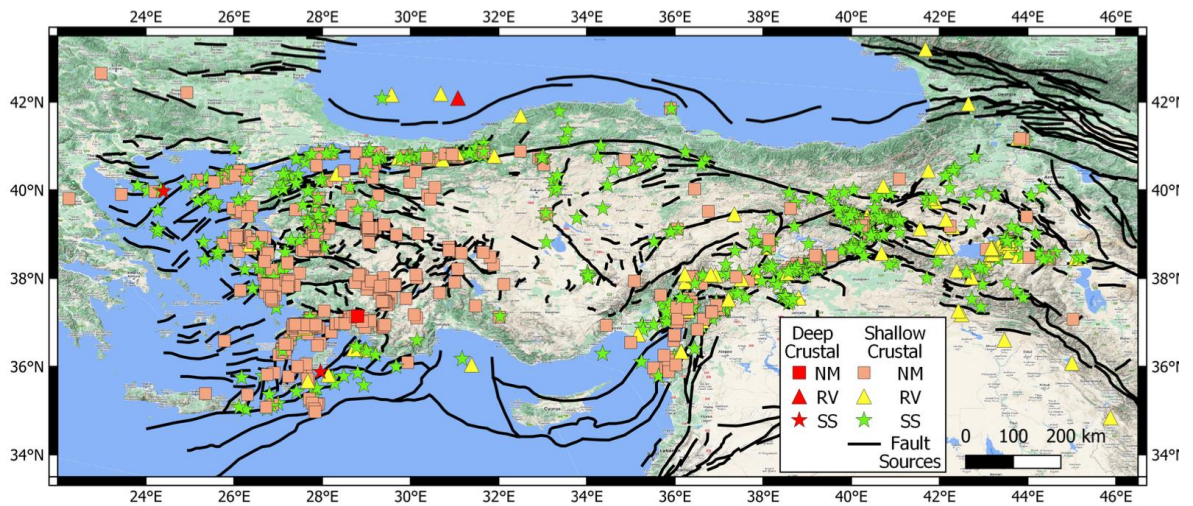
Figure 4.4. Geograpic distribution of crustal events in terms of SoF and focal depth. The boundary of shallow and deep active crustal earthquakes is 35 km.
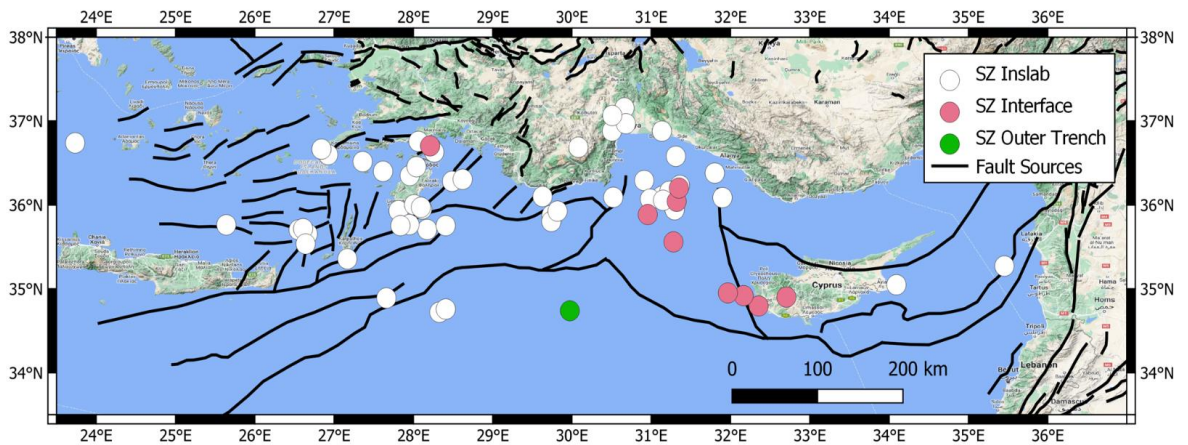
Figure 4.5. Geograpic distribution of subduction events
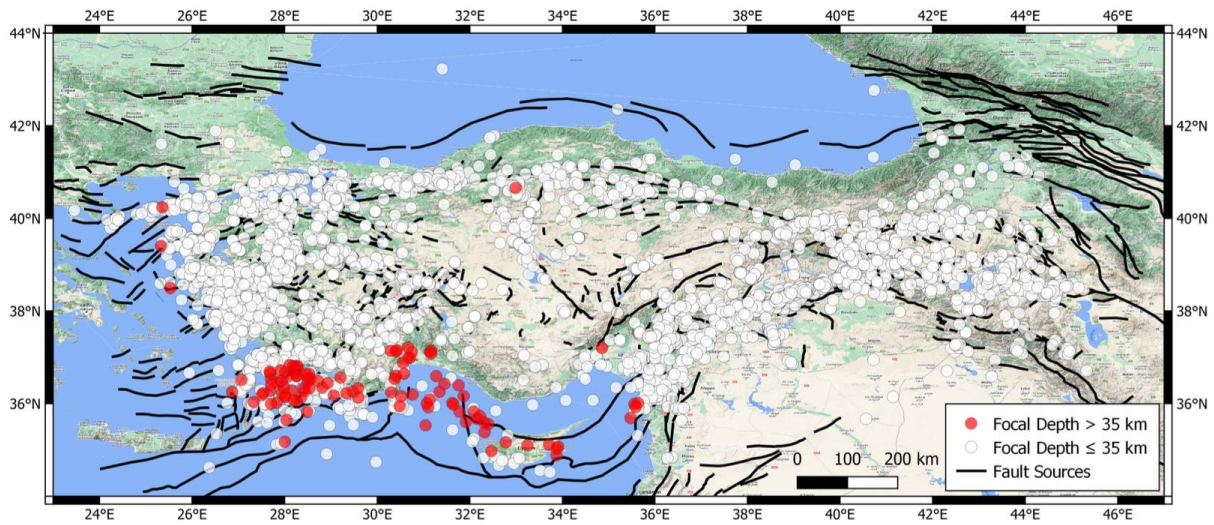
Figure 4.6. Geograpic distribution of events without moment tensor solution or M_w.

The majority of moderate-to-large magnitude earthquakes in the database are concentrated in the western part of Türkiye, particularly along the strike-slip North Anatolian Fault (NAF) and the extensional regime characterized by normal earthquakes in the Aegean region. The large magnitude events from the Eastern Anatolian Fault (EAF), which is dominated by strike-slip earthquakes, are mostly from the last two decades. Mainshocks and their aftershocks from the western part of Türkiye constitute 46% of the database, followed by events from Eastern Türkiye (29%, associated with the EAF system). The NAF accounts for 10% of the accelerometric data, and 14% of the accelerograms in SMD-TR are from the Mediterranean region. Only 1% of the events in the database are from the Hellenic and Cyprus Arcs, which are associated with subduction events. These figures provide valuable insights into the seismic activity and tectonic settings of Türkiye.

Figure 4.7 provides histograms displaying the distributions of events (left column panels) and accelerograms (right column panels) based on various seismic parameters.
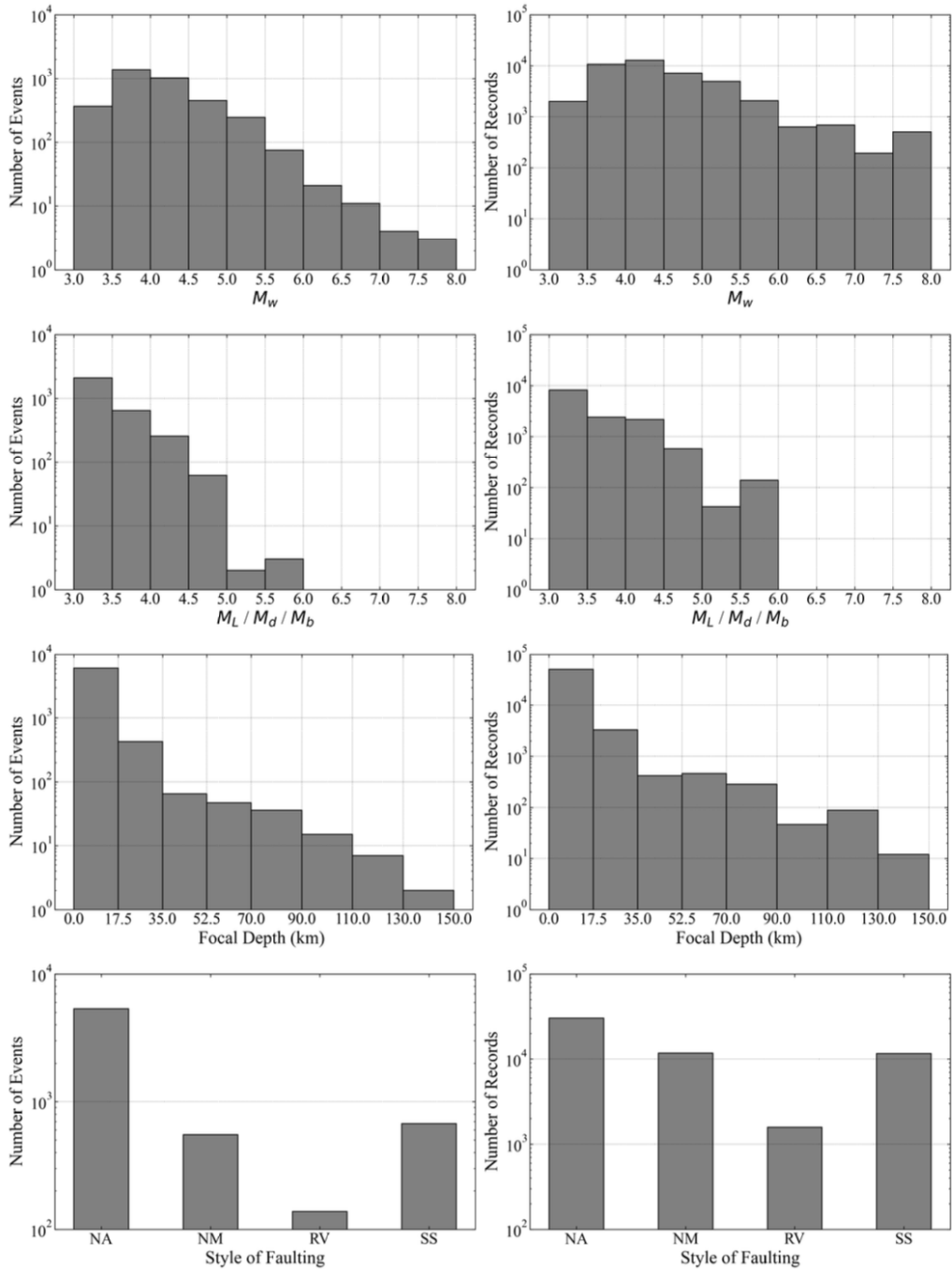
Figure 4.7. Histograms for event information. The top panel shows magnitudes in any
scale. The acronyms are NA: not available, NM: normal, RV: reverse and SS:
strike-slip.

The top row presents the distribution of events and accelerograms by moment magnitude
(M_w). It reveals that 96.8% of the events have $M_w \leq 5.5$, which corresponds to 90.2% of
the accelerometric data. Only 6.5% of the processed records fall within the M_w range of

5.5 to 6.5 (representing 2.7% of the events), and 3.3% of the processed data have M_w greater than 6.5, accounting for 0.5% of the data with reported M_w.

The second row illustrates the distribution of magnitudes in other scales. Notably, there are no events with magnitudes larger than 5.7, and only 5 events have magnitudes between 5 and 5.7, constituting 1.3% of the records.

The third row depicts the distribution of events and accelerograms based on focal depth. The majority of events (94%) are shallow crustal earthquakes with focal depths less than 20 km, which also make up 95% of the accelerograms.

The bottom row focuses on the style-of-faulting (SoF). It should be noted that there is no SoF information available for 5,349 earthquakes out of 6,710, representing 54.8% of the records. Among earthquakes with available SoF information, 49% are classified as strike-slip, while 41% are categorized as normal SoF. Strike-slip and normal events each constitute 94% of the accelerograms (with a 47% share for each). Reverse events make up only 10% of the earthquakes, and 6% of the records correspond to this SoF. These histograms provide a detailed overview of the seismic characteristics within the SMD-TR database.

Figure 4.8 presents scatter diagrams depicting the distribution of moment magnitude (M_w) in relation to distance metrics for different styles of faulting (SoF) within the SMD-TR. Here's a breakdown of the scatter diagrams:

- The top-left panel displays the scatter diagram for normal faulting earthquakes.
- The top-right panel shows the scatter diagram for reverse faulting earthquakes.
- The bottom-left panel depicts the scatter diagram for strike-slip faulting earthquakes.
- The bottom-right panel illustrates the scatter diagram for records with unknown SoF and fault-plane solution, for which the R_{epi} distance metric is used.
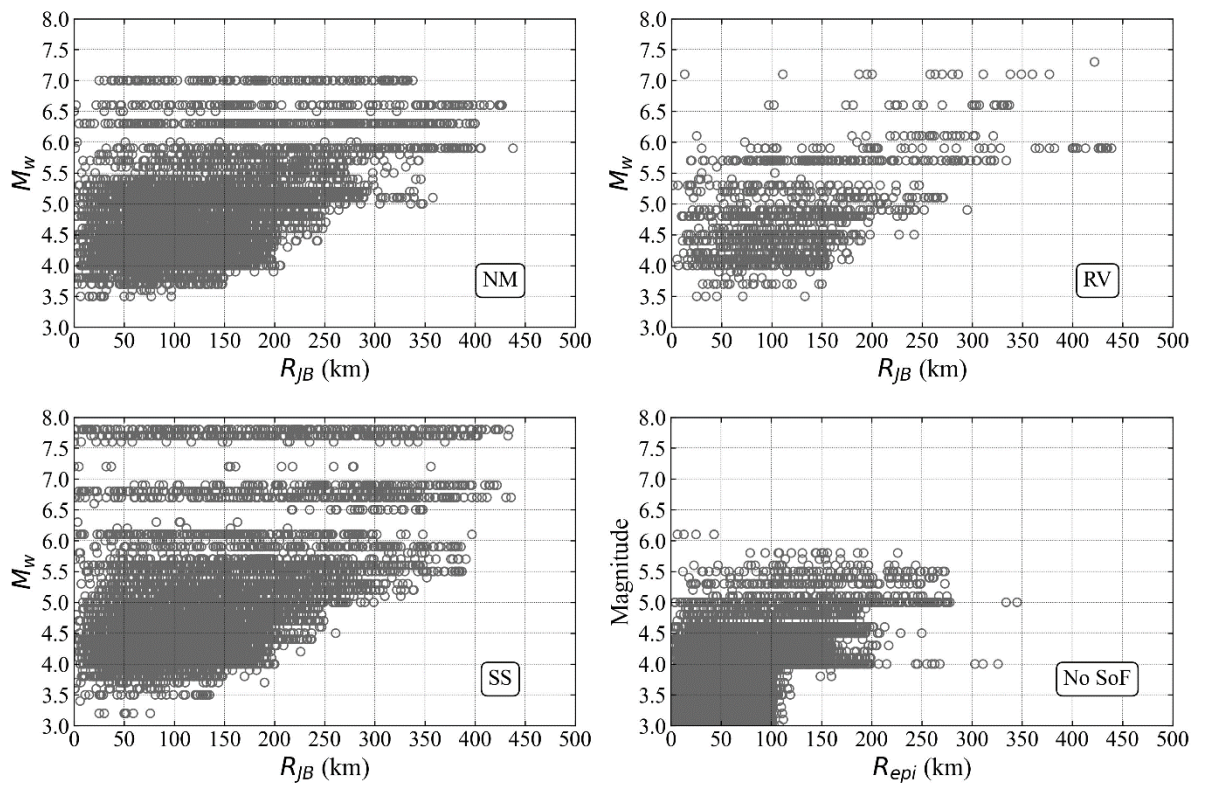
Figure 4.8. Magnitude-distance scatters for dip-slip (normal and reverse earthquakes), strike-slip earthquakes and events without SoF information.

These scatter diagrams reveal several important insights:

- Records are well-sampled for earthquakes with M_w less than 5.5.
- There is a noticeable magnitude gap ($6 \leq M_w \leq 7$) for reverse faulting events. This suggests a limited number of data points in this magnitude range for reverse faulting earthquakes.
- While scatter diagrams for normal and strike-slip events hint at a similar gap, it is not as pronounced as in the case of reverse faulting events.

These diagrams provide a visual representation of the distribution of earthquake magnitudes concerning their associated distance metrics, which can be valuable for seismic hazard assessment and modelling.

Figure 4.9 provides an overview of the spatial distribution of the 974 stations within the SMD-TR dataset. A breakdown of the information presented in this figure:

- Blue triangles represent stations with measured V_{S30} values.
- Brown triangles represent stations without measured V_{S30} values.
- There are 160 inactive stations, and 133 of them have measured V_{S30} information.
- There are 814 active stations, and 512 of them have site measurements, including V_{S30} data.
- Stations with measured V_{S30} values constitute 73% of the entire database.
- On average, there are approximately 80 recordings per station in the dataset.

Figure 4.10 offers a more detailed breakdown of the number of stations and recordings in terms of V_{S30} intervals. The histograms show the distribution of stations and recordings across different V_{S30} categories. Notably, about two-thirds of the records correspond to sites with soft-to-stiff soil conditions ($V_{S30} < 500$ m/s).

Figure 4.11 displays a scatter diagram illustrating the relationship between V_{S30} and Z1. As expected, an increase in V_{S30} is associated with a decrease in the depth-to-rock (Z1). This relationship is a fundamental consideration in seismic site characterization and hazard assessment, as soil conditions play a significant role in ground motion amplification during earthquakes.

Additionally, the plot indicates that for low-V_{S30} sites, the Vs profiles may not reach the 1 km/s horizon, making it challenging to model a proper V_{S30}-Z1 relation for Türkiye at these specific locations.
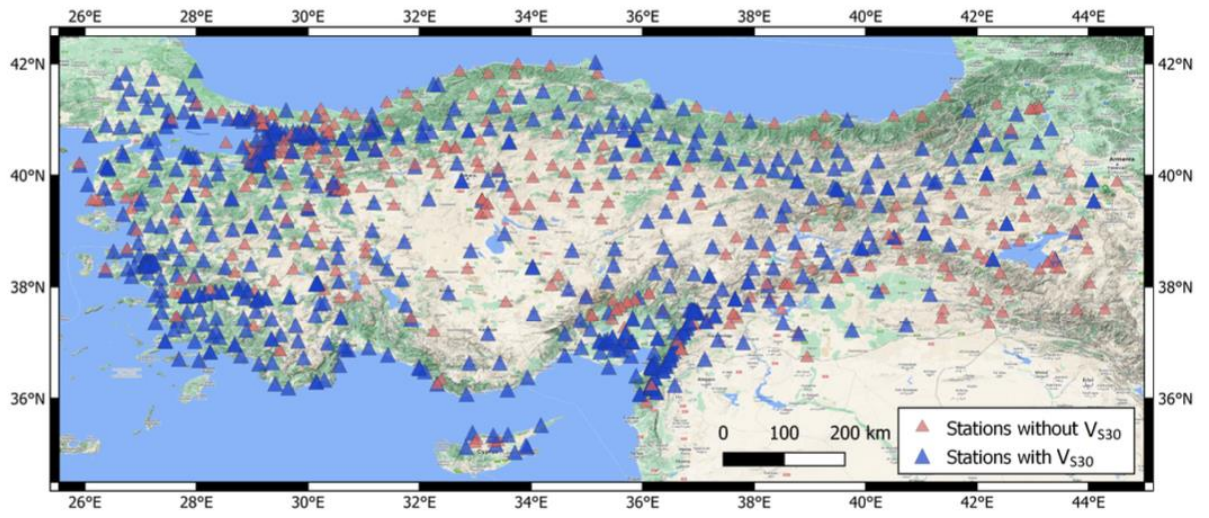
Figure 4.9. Geographic distribution of the strong-motion recording stations in Türkiye.
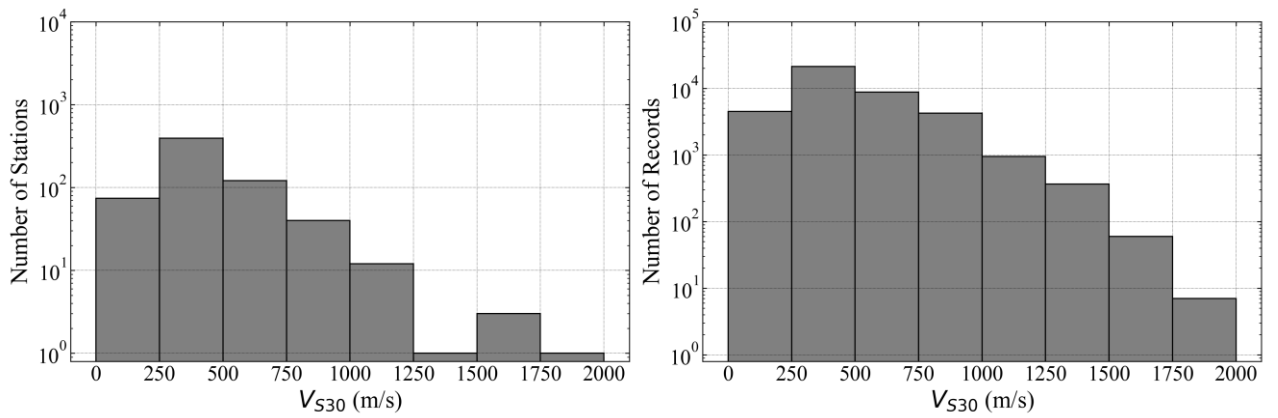
Figure 4.10. Histograms for site information.
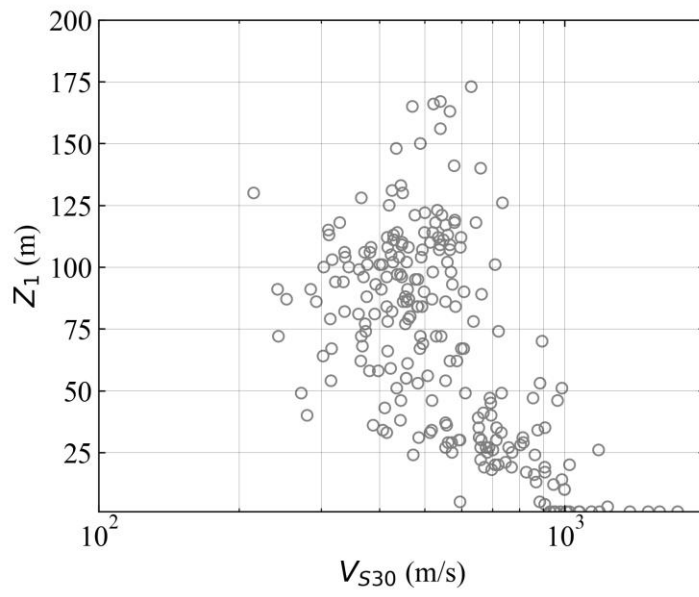
Figure 4.11. Scatter distribution of V_{S30}-Z1

5. CONCLUDING REMARKS

5.1. Summary

An updated edition of the Strong-Motion Database of Türkiye (SMD-TR) was created, which includes seismic data from 9,244 earthquakes spanning the period from 1976 to February 28th, 2023. This revised database encompasses 95,890 three-component recordings collected from 1,022 stations. The compilation process adheres to the latest methods, ensuring the accuracy and comprehensiveness of metadata, including event locations, moment magnitudes, rupture fault features, and dimensions. Additionally, the style of faulting was determined, earthquakes were categorized into classes, and aftershocks were identified. Site characterization relies on shear wave velocity profiles, particularly focusing on V_{s30} and Z1 values when available. Waveform processing encompasses both manual and automatic methods, involving a total of 55,375 records from 974 stations and 6710 events. The database also includes essential information such as peak ground motions, response spectra, and ground-motion duration for these waveforms. It's important to note that this database is publicly accessible via DesignSafe (https://doi.org/10.17603/ds2-f21x-s189).

5.2. Conclusion

The main conclusions of this study are listed below:

- Compared to Akkar et al. 2010, SMD-TR increases the usable number of recordings in the database. This is linked to the expansion of the station network. In Akkar et al. 2010, there were 1673 processed records, while this study provides 55375 processed records.

- Both V_{s30} and moment tensor solutions (style-of-faulting, distance computations, etc.) are crucial for developing GMPEs, since they are the main predictors variables. Missing such values for records renders approximately half of the database. This can play a major role in generating ground motion models.

- The automatic algorithm proposed by the study yield acceptable results, with its limitations offset by the number of records it provides to the database. While modifications and other methods for fast processing

37

should be studied in the future, automatic processing algorithms are a necessity at the current state of Turkish Strong-motion Network. It should be highlighted again that the efficiency of the APS is limited to the magnitude range it was designed and tested for, and at this current stage, it should not be preferred over MPS for high magnitude events.

- The equation for magnitude dependent $f_{low\text{-}cut}$ shows promising results, showing similar results with manually processed records in this study and previous Türkiye Databases. The results are also similar to NGA-West2 averages for Magnitudes M5.0- and M6.5+. The proposed equation is safe to use for low magnitude events, and it's sufficient for quick solutions for high magnitude events.

5.3. Possible Extensions for the Database

There are two main parts of possible expansions for the database, that are either to increase the overall efficiency of the automatic process, or to address other uncertainty problems in database development. These points will mostly be studied or applied in the future depending on their effectiveness and was ruled out of the scope of this thesis due to time limitations.

- The current preprocessing algorithm is good at avoiding false-positive flagging of bad quality records. Despite its success, it also misses a substantial number of records that should have been eliminated. Currently these records are a small percentage in the overall state of the database and are mostly limited to multi-wave records with similar peaks. This increase in error is due to the method applied to detect multi-wave records being dependent on up-to-date small magnitude databases, which isn't perfect for immediate aftershocks after high magnitude earthquakes. There are several different options to address this issue, such as flagging records with high significant duration time values, but details and results of such methods are yet to be investigated.

- One of the main problems of correct distance metrics is the uncertainty in the moment tensor solutions of the earthquakes, and the epicenter location. While these parameters are taken as they are given from the sources as preferred values, the uncertainty related to the parameters (e.g., R_{rup}) should be calculated.

- While M5.5+ is a good separation limit for automatic processing and manual processing of records, records with M5.0+ can still be considered valuable records for engineering purposes. Future updates of the database can reduce the limit from M5.5 to M5.0.

REFERENCES

Akkar, S., Bommer, J.J., Influence of long-period filter cut-off on elastic spectral displacements. Earthq Eng Struct Dyn 35:1145–1165, **2006.**

Akkar, S., Çagnan, Z., Yenier, E., Erdogan, Ö., Sandıkkaya, M.A., Gülkan, P., The recently compiled Turkish strong-motion database: preliminary investigation for seismological parameters. J Seismol 14:457–479, **2010.**

Akkar, S., Kale O., Yenier, E., Bommer, J.J., The high-frequency limit of usable response spectral ordinates from filtered analogue and digital strong-motion accelerograms. Earthq Eng Struct Dyn 40:1387–1401, **2011.**

Akkar, S., Kale, Ö., Yakut, A. et al., Ground-motion characterization for the probabilistic seismic hazard assessment in Turkey. Bull Earthquake Eng 16, 3439–3463, **2018.**

Akkar, S., Sandıkkaya, M.A., Şenyurt, M., A., Azari Sisi, Ay, B.Ö., Traversa, P., Douglas, J., Cotton, F., Luzi, L., Hernandez B., and Godey, S., Reference database for seismic ground-motion in Europe (RESORCE). Bulletin of earthquake engineering 12 (1): 311-339., **2014.**

Aksarı, D., Karabulut, H. and Özalaybey, S., Stress interactions of three moderate size earthquakes in Afyon, southwestern Turkey. Tectonophysics, 485(1-4), pp.141-153., **2009.**

Aktar, M., Ergin, M., Özalaybey, S., Tapirdamaz, C., Yörük, A. and Biçmen, F., A lower-crustal event in the northeastern Mediterranean: The 1998 Adana earthquake (Mw= 6.2) and its aftershocks. Geophysical Research Letters, 27(16), pp.2361-2364., **2000.**

Alipour, N., Sandıkkaya, M.A., and Gülerce, Z., Ground motion characterization for vertical ground motions in Turkey—Part 1: V/H ratio ground motion models. Pure and Applied Geophysics 177 (5): 2083-2104, **2020.**

Ambraseys, N.N., Smit, P, Douglas, J, Margaris, B, Sigbjörnsson, R, Olafsson, S, Suhadolc, P, Costa, G, Internet site for European strong-motion data. Bollettino di Geofisica Teorica ed Applicata 45:113–129, **2004.**

Ancheta, T.D., Darragh, R.B., Stewart, J.P., Seyhan, E., Silva, W.J., Chiou, B.S.J., Wooddell, K.E., Graves, R.W., Kottke, A.R., Boore D.M., and Kishida., T., NGA-West2 database. Earthquake Spectra 30 (3): 989-1005., **2014.**

Anderson, J., Zeng, Y. and Sucuoglu, H., Analysis of Accelerations from the 1 October 1995 Dinar, Turkey, Earthquake. Bulletin of the Seismological Society of America, 91(6), pp.1433-1445., **2001.**

Atkinson, G.M., Silva, W., Stochastic modeling of California ground motions. Bull Seismol Soc Am 90:255–274, **2000.**

Bahrampouri, M., Rodriguez-Marek, A., Shahi, S., & Dawood, H., An updated database for ground motion parameters for KiK-net records. Earthquake Spectra, 37(1), 505-522., **2001.**

Bernard, P., Gariel, J. and Dorbath, L., Fault location and rupture kinematics of the magnitude 6.8, 1992 Erzincan earthquake, Turkey, from strong ground motion and regional records. Bulletin of the Seismological Society of America, 87(5), pp.1230-1243., **1997.**

Bondár, I. and Storchak, D.A., Improved location procedures at the International Seismological Centre, Geophys. J. Int., 186, 1220-1244., **2011.**

Boore, D.M., Atkinson, G.M., Boore–Atkinson NGA ground motion relations for the geometric mean horizontal component of peak and spectral ground motion parameters. In: PEER2007/01, Pacific earthquake engineering research center, University of California, Berkeley, CA, **2007.**

Boore, D.M., Azari Sisi, A, Akkar S., Using pad-stripped acausally filtered strong-motion data. Bull Seismol. Soc. Am. 102:751–760, **2012.**

Boore, D.M., Bommer, J.J., Processing of strong-motion accelerograms? Needs, options and consequences. Soil Dyn Earthq Eng 25:93–115, **2005.**

Boore, D. M., Orientation-independent, nongeometric-mean measures of seismic intensity from two horizontal components of motion. Bull. Seism Soc Am, 100:1830-1835. **2010.**

Boore, D. M. and S. Akkar, Effect of causal and acausal filters on elastic and inelastic response spectra, Earthq. Eng. and Struct. Dynamics 32, 1729-1748. **2003.**

Boore, D. M., A. Azari Sisi, and S. Akkar, Using pad-stripped acausally filtered strong-motion data, Bull. Seismol. Soc. Am. 102 751-760. **2012.**

Brune, J.N., Tectonic stress and the spectra of seismic shear waves from earthquakes, Journal of Geophysical Research, 75(26), pp. 4997–5009, **1970.**

Contreras, V., J.P., Stewart, T., Kishida, R.B., Darragh, B.S., Chiou, S., Mazzoni, R.R., Youngs, N.M., Kuehn, S.K., Ahdi, K., Wooddell, and R., Boroschek, NGA-Sub source and path database. Earthquake Spectra, 38 (2): 799-840., **2022.**

Danciu, L., Kale, Ö. and Akkar, S., The 2014 Earthquake Model of the Middle East: ground motion model and uncertainties. Bull Earthquake Eng 16, 3497–3533, **2018.**

Dawood, H.M., Rodriguez-Marek, A., Bayless, J., Goulet, C., and Thompson, E., A flatfile for the KiK-net database processed using an automated protocol. Earthquake Spectra 32 (2): 1281-1302., **2016.**

Delouis, B., Lundgren, P., Salichon, J. and Giardini, D., Joint inversion of InSAR and teleseismic data for the slip history of the 1999 Izmit (Turkey) Earthquake. Geophysical Research Letters, 27(20), pp.3389-3392., **2011.**

Di Giacomo, D., Engdahl, E.R. and Storchak, D.A., The ISC-GEM Earthquake Catalogue (1904–2014): status after the Extension Project, Earth Syst. Sci. Data, 10, 1877-1899., **2018.**

Di Giacomo, D., Storchak, D.A., Safronova, N., Ozgo, P., Harris, J., Verney, R. and Bondár, I., A New ISC Service: The Bibliography of Seismic Events, Seismol. Res. Lett., 85, 2, 354-360, **2014.**

Doğan, B., Irmak, T., Karakaş, A. and Kalafat, D., Seismotectonic content by the source parameters of the 10 June 2012 Ölüdeniz-Fethiye (Dodecanese Islands) Mw 6.1 earthquake and aftershocks (southwestern Turkey). Acta Geodaetica et Geophysica, 51(1), pp.15-41. **2015.**

Donahue, J.L. and Abrahamson, N.A., Simulation-based hanging wall effects, Earthquake Spectra, 30(3), pp. 1269–1284. **2014.**

Douglas, J., What is poor quality strong-motion record? Bull Earthq Eng 1:141–156, **2003.**

Douglas, J. and Boore, D. M., High-frequency filtering of strong-motion records, Bull. Earthquake Engineering 9 395-409., **2011.**

Engdahl, E. R., Di Giacomo, D., Sakarya, B., Gkarlaouni, C. G., Harris, J., and Storchak, D. A., ISC-EHB 1964-2016, an Improved Data Set for Studies of Earth Structure and Global Seismicity, Earth and Space Science, 7(1), e2019EA000897, **2020.**

Erdik, M., Report on the Turkish Earthquake of October 30, 1983. Earthquake Spectra, 1(1), pp.151-172. **1984.**

Ergin, M., Aktar, M. and Eyidogan, H., Present-day seismicity and Seismotectonics of the Cilician Basin: Eastern Mediterranean region of Turkey, Bulletin of the Seismological Society of America, 94(3), pp. 930–939., **2004.**

Ganas, A., Elias, P., Briole, P., Valkaniotis, S., Escartin, J., Tsironi, V., Karasante, I. and Kosma, C., Co-seismic and post-seismic deformation, field observations and fault model of the 30 October 2020 Mw = 7.0 Samos earthquake, Aegean Sea. Acta Geophysica, 69(3), pp.999-1024., **2021.**

Ganas, A., Elias, P., Kapetanidis, V., Valkaniotis, S., Briole, P., Kassaras, I., Argyrakis, P., Barberopoulou, A. and Moshou, A., The July 20, 2017, M6.6 Kos Earthquake: Seismic and Geodetic Evidence for an Active North-Dipping Normal Fault at the Western End of the Gulf of Gökova (SE Aegean Sea). Pure and Applied Geophysics, 176(10), pp.4177-4211., **2019.**

Garcia, D, Wald, D.J. and Hearne M.G., A global earthquake discrimination scheme to optimize ground-motion prediction equation selection. Bulletin of the Seismological Society of America 102(1): 185–203., **2012.**

Gardner, J. K., and Knopoff, L., Is the sequence of earthquakes in Southern California, with aftershocks removed, Poissonian?,Bull. Seism. Soc. Am. 64 1363-1367., **1974.**

Gombert, B., Duputel, Z., Shabani, E., Rivera, L., Jolivet, R. and Hollingsworth, J., Impulsive Source of the 2017MW=7.3 Ezgeleh, Iran, Earthquake. Geophysical Research Letters, 46(10), pp.5207-5216. **2019.**

Goulet, C.A., Bozorgnia, Y., Kuehn, N., Al Atik, L., Youngs, R.R., Graves, R.W., and Atkinson., G.M., NGA-East ground-motion characterization model Part I: Summary of products and model development. Earthquake Spectra, 37 (1_suppl): 1231-1282., **2021.**

Hayes, G. P., Moore, G. L., Portner, D. E., Hearne, M., Flamme, H., Furtney, M., & Smoczyk, G. M., Slab2, a comprehensive subduction zone geometry model. Science, 362(6410), 58-61. **2018.**

Howell, A., Jackson, J., Copley, A., McKenzie, D. and Nissen, E., Subduction and vertical coastal motions in the eastern Mediterranean. Geophysical Journal International, 211(1), pp.593-620. **2017.**

International Seismological Centre, ISC-EHB dataset, https://doi.org/10.31905/PY08W6S3, **2023.**

International Seismological Centre, https://doi.org/10.31905/D808B830, **2023.**

Kagan, Y.Y., Seismic moment distribution revisited: I. Statistical results. Geophysical Journal International 148(3): 520–541, **2002.**

Kalafat, D., Kekovalı, K. and Pınar, A., Source Characteristics of the January 8, 2013 (Mw = 5.7) and May 24, 2014 (Mw = 6.8) North Aegean Earthquakes Sequence. Moment Tensor Solutions, pp.339-376. **2018.**

Kalafat, D., Kekovalı, K., Akkoyunlu, F. and Ögütçü, Z., Source mechanism and stress analysis of 23 October 2011 Van Earthquake (Mw = 7.1) and aftershocks. Journal of Seismology, 18(3), pp.371-384., **2013.**

Karabulut, H., Güvercin, S., Eskiköy, F., Konca, A., & Ergintav, S., The moderate size 2019 September Mw 5.8 Silivri earthquake unveils the complexity of the Main Marmara Fault shear zone. Geophysical Journal International, 224(1), 377-388., **2020.**

Kartal, R. F., Demirtaş, R., Kadirioğlu, F. T., Seismotectonic Evaluation of August 08, 2019 Bozkurt (Denizli) Earthquake (Mw 6.0): Western Turkey, AFAD, Deprem Dairesi Başkanlığı, Ankara, Türkiye., **2019.**

Kiratzi, A. and Louvari, E., Focal mechanisms of shallow earthquakes in the Aegean Sea and the surrounding lands determined by waveform modelling: A new database, Journal of Geodynamics, 36(1-2), pp. 251–274., **2003.**

Koller, M., robustlmm: an R package for robust estimation of linear mixed-effects models. J Stat Softw 75:1-24., **2016.**

Kurtulus, C., Sertcelik, F., Sertcelik, I., Kuru, T., Tekin, K., Ates, E., Apak, A., Kokbudak, D., Sezer, S., Yalcin, D., Determination of site characterization in Turkey strong motion recording stations. Journal of the Faculty of Engineering and Architecture of Gazi University 35(4), 1829- 1846., **2020.**

Lanzano, G., Luzi, L., Cauzzi, C., Bienkowski, J., Bindi, D., Clinton, J., ... & Theodoulidis, N., Accessing European strong-motion data: An update on ORFEUS coordinated services. Seismological Research Letters, 92(3), 1642-1658., **2021.**

Lentas, K., Di Giacomo, D., Harris, J., and Storchak, D. A., The ISC Bulletin as a comprehensive source of earthquake source mechanisms, Earth Syst. Sci. Data, 11, 565-578, **2019.**

Ozalaybey, S., The 1999 Izmit earthquake sequence in Turkey: Seismological and tectonic aspects, Bulletin of the Seismological Society of America, 92(1), pp. 376–386., **2002.**

Papadimitriou, P., Kassaras, I., Kaviris, G., Tselentis, G., Voulgaris, N., Lekkas, E., Chouliaras, G., Evangelidis, C., Pavlou, K., Kapetanidis, V., Karakonstantis, A., Kazantzidou-Firtinidou, D., Fountoulakis, I., Millas, C., Spingos, I., Aspiotis, T., Moumoulidou, A., Skourtsos, E., Antoniou, V., Andreadakis, E., Mavroulis, S. and Kleanthi, M., The 12th June 2017 Mw = 6.3 Lesvos earthquake from detailed seismological observations. Journal of Geodynamics, 115, pp.23-42., **2018.**

Papadopoulos, G., Agalos, A., Karavias, A., Triantafyllou, I., Parcharidis, I. and Lekkas, E., Seismic and Geodetic Imaging (DInSAR) Investigation of the March 2021 Strong Earthquake Sequence in Thessaly, Central Greece. Geosciences, 11(8), p.311., **2021.**

Polat, O., The Izmit (Kocaeli), Turkey earthquake of 17 August 1999: Previous seismicity, aftershocks, and Seismotectonics, Bulletin of the Seismological Society of America, 92(1), pp. 361–375., **2002.**

Rennolet, S. B., Moschetti, M. P., Thompson, E. M., & Yeck, W. L., A flatfile of ground motion intensity measurements from induced earthquakes in Oklahoma and Kansas. Earthquake Spectra, 34(1), 1-20., **2018.**

Russo, E., Felicetta, C., D Amico, M., Sgobba, S., Lanzano, G., Mascandola, C., Pacor, F., Luzi, L., Italian Accelerometric Archive v3.2 - Istituto Nazionale di Geofisica e Vulcanologia, Dipartimento della Protezione Civile Nazionale., **2022.**

Saltogianni, V., Gianniou, M., Taymaz, T., Yolsal-Çevikbilen, S. and Stiros, S., Fault slip source models for the 2014 Mw 6.9 Samothraki-Gökçeada earthquake (North Aegean Trough) combining geodetic and seismological observations. Journal of Geophysical Research: Solid Earth, 120(12), pp.8610-8622., **2015.**

Sandıkkaya et al., An Updated Strong-Motion Database of Türkiye (SMD-TR). DesignSafe Data Depot. https://doi.org/10.17603/ds2-f21x-s189, **2023.**

Sandıkkaya, M.A., Yılmaz, M.T., Bakır, B.S., Yılmaz. Ö., Site classification of Turkish national strong-motion stations. J Seismol 14:543–563, **2010.**

Scordilis, E., Theodoulidis, N., Kalogeras, I., Margaris, B., Klimis, N., Skarlatoudis, A., Stewart, J., Boore, D., Seyhan, E., Savvaidis, A., Mylonakis, G., and Pelekis, P., Strong motion database for crustal earthquakes in Greece and surrounding area, Proceedings, 16th European Conference on Earthquake Engineering, Thessaloniki, Greece, 18--21 June, 2018 (accepted), **2018.**

Shahi, S.K. and Baker, J.W., NGA-West2 models for ground motion directionality. Earthquake Spectra, 30(3), 1285-1300., **2014.**

Sözbilir, H., Tatar, O., Çakır, R., Eski, S., Softa, M., Duran, İ., Akgün, M., Utku, M. Koçbulut., F, 14 Haziran 2020 Bingöl-Karliova Depremi Ön İnceleme Raporu, Dokuz Eylül Üniversitesi Deprem Araştırma ve Uygulama Merkezi, Diri Fay Araştırma Grubu, **2020.**

Storchak, D.A., Harris, J., Brown, L., Lieser, K., Shumba, B., Di Giacomo, D., Rebuild of the Bulletin of the International Seismological Centre (ISC)—part 2: 1980–2010. Geosci. Lett. 7: 18, **2020.**

Tan, O. and Taymaz, T., Active tectonics of the Caucasus: Earthquake source mechanisms and rupture histories obtained from inversion of teleseismic body waveforms. Postcollisional Tectonics and Magmatism in the Mediterranean Region and Asia., **2006.**

Tan, O., Pabuçcu, Z., Tapırdamaz, M., İnan, S., Ergintav, S., Eyidoğan, H., Aksoy, E. and Kuluöztürk, F., Aftershock study and seismotectonic implications of the 8 March 2010 Kovancılar (Elazığ, Turkey) earthquake (MW= 6.1). Geophysical Research Letters, 38(11), **2011.**

Taymaz, T., Eyidoğan, H. and Jackson, J., Source parameters of large earthquakes in the East Anatolian Fault Zone (Turkey). Geophysical Journal International, 106(3), pp.537-550., **1991.**

Taymaz, T., Ganas, A., Berberian, M., Eken, T., Irmak, T., Kapetanidis, V., Yolsal-Çevikbilen, S., Erman, C., Keleş, D., Esmaeili, C., Tsironi, V. and Özkan, B., The 23

February 2020 Qotur-Ravian earthquake doublet at the Iranian-Turkish border: Seismological and InSAR evidence for escape tectonics. Tectonophysics, 838, p.229482., **2022.**

Taymaz, T., Ganas, A., Yolsal-Çevikbilen, S., Vera, F., Eken, T., Erman, C., Keleş, D., Kapetanidis, V., Valkaniotis, S., Karasante, I., Tsironi, V., Gaebler, P., Melgar, D. and Öcalan, T., Source Mechanism and Rupture Process of the 24 January 2020 Mw 6.7 Doğanyol–Sivrice Earthquake obtained from Seismological Waveform Analysis and Space Geodetic Observations on the East Anatolian Fault Zone (Turkey). Tectonophysics, 804, p.228745., **2021.**

Triantafyllou, I., Karavias, A., Koukouvelas, I., Papadopoulos, G. and Parcharidis, I., The Crete Isl. (Greece) Mw6.0 Earthquake of 27 September 2021: Expecting the Unexpected. GeoHazards, 3(1), pp.106-124., **2022.**

Umutlu, N., Koketsu, K. and Milkereit, C., The rupture process during the 1999 Düzce, Turkey, earthquake from joint inversion of teleseismic and strong-motion data. Tectonophysics, 391(1-4), pp.315-324., **2004.**

Vannucci, G. and P., Gasperini, P., The new release of the database of earthquake mechanisms of the Mediterranean area (Emma Version 2), Annals of Geophysics, 47(1 Sup.)., **2009.**

Wang, P., Stewart, J. P., Bozorgnia, Y., Boore, D. M., & Kishida, T. R package for computation of earthquake ground motion response spectra. Pacific Earthquake Engineering Center, Report 2017/09., **2017.**

Wiemer, S. A Software Package to Analyze Seismicity: ZMAP. Seismological Research Letters, 72, 373-382., **2001.**

Yang, J., Xu, C., Wang, S. and Wang, X., Sentinel-1 observation of 2019 Mw 5.7 Acipayam earthquake: A blind normal-faulting event in the Acipayam basin, southwestern Turkey. Journal of Geodynamics, 135, p.101707., **2020.**

Yenier E., Sandıkkaya, M.A., Akkar. S., Report on the fundamental features of the extended strong motion databank prepared for the SHARE project, pp. 44. Deliverable 4.1 of Seventh Framework Programme Project Seismic Hazard Harmonization in Europe (SHARE), 34 pages, Ankara, **2010.**

Yolsal-Çevikbilen, S. and Taymaz, T., Earthquake source parameters along the Hellenic subduction zone and numerical simulations of historical tsunamis in the Eastern Mediterranean. Tectonophysics, 536-537, pp.61-100., **2012.**

Yolsal-Çevikbilen, S., Taymaz, T. and Helvacı, C., Earthquake mechanisms in the Gulfs of Gökova, Sığacık, Kuşadası, and the Simav Region (western Turkey): Neotectonics, seismotectonics and geodynamic implications. Tectonophysics, 635, pp.100-124., **2014.**

Zahradnik, J., The Weak-Motion Modeling of the Skyros Island, Aegean Sea, M w = 6.5 Earthquake of July 26, 2001. Studia Geophysica et Geodaetica, 46(4), pp.753-771., **2002.**

APPENDIX

APPENDIX 1 – Event Information Compiled from Literature Survey

EQID	UTC Time	Latitude	Longitude	Depth (km)	Moment Magnitude	Style-of-Faulting	Strike	Dip	Rake	Fault Plane Solution Refferrence
1	1976-08-19T01:12:39.000000Z	37.7510	29.0120	15	5.3	NM	164	45	-30	Kiratzi_&_Louvari_(2003)
4	1977-12-16T07:37:29.300000Z	38.3790	27.2040	15	5.5	NM	304	70	-76	Vanucci_and_Gasperini_(2004)
11	1983-10-30T04:12:28.100000Z	40.3500	42.1940	15	6.6	SS	38	73	-17	Erdik_(1984)
16	1986-05-05T03:35:38.000000Z	38.0370	37.7700	10	6.1	RV	273	49	31	Taymaz_et_al._(1991)
18	1986-06-06T10:39:47.000000Z	38.0490	37.9020	10	5.9	RV	275	27	30	Taymaz_et_al._(1991)
23	1992-03-13T17:18:39.400000Z	39.7060	39.6000	20	6.7	SS	124	90	175	Bernard_et_al._(1997)
72	1995-04-13T20:23:15.600000Z	37.4470	36.2250	15	4.8	NM	170	40	-90	Ergin_et_al._(2004)
86	1995-10-01T15:57:13.100000Z	38.0090	30.1400	15	6.5	NM	149	45	-87	Anderson_et_al._(2001)
199	1997-01-23T14:53:12.900000Z	36.2057	35.9819	7	4.2	SS	45	85	-40	Ergin_et_al._(2004)
334	1998-06-27T13:55:00.000000Z	36.9410	35.2570	20	6.2	SS	65	90	5	Aktar_et_al._(2000)
425	1999-01-15T02:04:30.290000Z	37.0620	35.7960	19	4.3	SS	35	75	-10	Ergin_et_al._(2004)
476	1999-08-17T00:01:39.070000Z	40.8070	29.9790	15	7.6	SS	-1	85	164	Delouix_et_al._(2001)
492	1999-08-17T03:14:03.150000Z	40.6890	30.5700	15	5.3	NM	192	34	-82	Kiratzi_&_Louvari_(2003)
493	1999-08-17T04:14:17.810000Z	40.7702	29.1333	13	4.6	SS	113	70	175	Ozalaybey_et_al._(2002)
500	1999-08-17T20:30:00.000000Z	40.7261	29.2776	10	4	SS	116	72	-167	Ozalaybey_et_al._(2002)
511	1999-08-20T20:12:42.500000Z	40.6584	29.0898	11	4.3	NM	110	70	-60	Ozalaybey_et_al._(2002)
533	1999-08-26T17:49:34.400000Z	40.7514	30.0278	12	4	SS	85	90	-178	Ozalaybey_et_al._(2002)
567	1999-09-04T10:31:00.180000Z	40.7441	29.9386	11	4.7	SS	53	80	-176	Ozalaybey_et_al._(2002)
574	1999-09-06T06:33:27.160000Z	40.7402	29.7263	13	4.1	RV	71	41	56	Ozalaybey_et_al._(2002)
594	1999-09-09T20:21:51.080000Z	40.7076	29.9686	11	3.8	NM	82	54	-142	Ozalaybey_et_al._(2002)
616	1999-09-20T21:28:00.990000Z	40.6290	27.6200	20	5.2	SS	149.84	87.94	-21.53	Polat_et_al._(2002)
670	1999-11-12T16:57:21.410000Z	40.8160	31.2000	14	7.2	SS	264	64	-172	Umutlu_et_al._(2004)
749	1999-12-03T17:06:54.700000Z	40.4680	42.3270	10	5.6	SS	226	73	1	Tan_and_Taymaz_(2006)
859	2000-05-27T07:49:29.700000Z	36.1052	35.2416	30	4.8	SS	65	45	-10	Ergin_et_al._(2004)
1131	2000-12-15T16:44:44.450000Z	38.4570	31.1830	12	6	NM	314	41	-100	Aksarı_et_al._(2009)
1159	2001-03-24T13:07:40.860000Z	40.8448	28.8367	10	3.9	SS	105	78	-170	Ozalaybey_et_al._(2002)
1192	2001-06-23T06:52:37.900000Z	35.7080	28.1730	50	5.7	SS	80	87	8	Yolsal-Çevikbilen_and_Taymaz_(2012)
1210	2001-07-26T00:21:00.000000Z	39.0510	24.2580	15	6.5	SS	150	70	10	Zahradnik_(2002)
1262	2002-01-22T04:53:54.600000Z	35.6550	26.6680	91	6.1	SS	4	41	175	Yolsal-Çevikbilen_and_Taymaz_(2012)
1263	2002-02-03T07:11:29.230000Z	38.5780	31.1560	15	6.5	NM	306	38	-70	Aksarı_et_al._(2009)
1267	2002-02-03T09:26:45.820000Z	38.6330	30.8720	11	5.8	NM	236	45	-58	Aksarı_et_al._(2009)
1655	2004-08-04T03:01:07.080000Z	36.8710	27.7610	10	5.4	NM	61	38	-99	Yolsal-Çevikbilen_et_al._(2014)
1745	2005-01-23T22:36:06.420000Z	35.8790	29.7420	30	5.7	SS	228	61	0	Howell_et_al._(2017)
1817	2005-10-17T09:46:56.730000Z	38.1950	26.6540	10	5.7	SS	233	79	179	Yolsal-Çevikbilen_et_al._(2014)
1827	2005-10-20T21:40:02.720000Z	38.1670	26.7590	10	5.7	SS	223	81	-178	Yolsal-Çevikbilen_et_al._(2014)
2185	2008-07-15T03:26:36.440000Z	35.9320	27.8120	52	6.1	SS	94	80	30	Yolsal-Çevikbilen_and_Taymaz_(2012)
2283	2010-03-08T02:32:29.960000Z	38.7870	40.0330	10	6.1	SS	54	80	-10	Tan_et_al._(2011)
2285	2010-03-08T07:47:37.440000Z	38.7190	40.1010	10	5.5	SS	231	84	-6	Tan_et_al._(2011)
2480	2011-04-01T13:29:43.810000Z	35.7040	26.5530	75	6.1	SS	138	69	11	Howell_et_al._(2017)
2510	2011-05-19T20:15:22.790000Z	39.1290	29.0730	10	5.8	NM	287	58	-94	Yolsal-Çevikbilen_et_al._(2014)
2876	2011-10-23T10:48:15.010000Z	38.7060	43.3430	15	5.6	RV	47.2	50.9	106.5	Kalafat_et_al._(2013)
2878	2011-10-23T10:56:56.230000Z	38.7480	43.3370	15	5.5	RV	221.3	33.5	122.9	Kalafat_et_al._(2013)
2884	2011-10-23T20:45:42.060000Z	38.5440	43.1610	15	6	RV	193.9	49.1	73.9	Kalafat_et_al._(2013)
2894	2011-10-25T14:55:06.000000Z	38.8050	43.6210	15	5.4	RV	264	53	68	Kalafat_et_al._(2013)
2957	2011-11-09T19:23:33.000000Z	38.4190	43.3300	10	5.7	SS	245.7	34.8	-0.1	Kalafat_et_al._(2013)
3347	2012-06-10T12:44:15.000000Z	36.3540	28.9460	30	6.1	SS	212	78	3	Doğan_et_al._(2014)
3412	2012-07-09T13:54:57.000000Z	35.5720	28.9430	25	5.7	SS	43	79	2	Howell_et_al._(2017)
3581	2013-01-08T14:16:07.000000Z	39.6660	25.5340	15	5.7	SS	138.7	88.4	-12.8	Kalafat_et_al._(2013)
4200	2013-12-28T15:21:03.000000Z	36.0430	31.3230	53	5.9	RV	293	28	75	Howell_et_al._(2017)
4300	2014-05-24T09:25:00.000000Z	40.2740	25.3850	15	6.9	SS	79	90	-178	Saltogianni_et_al._(2015)
4729	2015-04-16T18:07:37.000000Z	35.1800	26.8450	24	6.1	RV	344	68	103	Howell_et_al._(2017)
5791	2017-06-12T12:28:37.000000Z	38.8740	26.3390	15	6.3	NM	122	40	-83	Papadimitriou_et_al._(2017)
5907	2017-07-20T22:31:09.000000Z	36.9680	27.4440	15	6.6	NM	283	37	-75	Ganas_et_al._(2019)
6255	2017-11-12T18:18:14.000000Z	34.8460	45.8760	20	7.3	RV	351	14	131	Gombert_et_al._(2018)
6900	2019-03-20T06:34:27.000000Z	37.4222	29.4959	7	5.7	NM	331.9	44.4	-76.2	Yang_et_al._(2020)
7095	2019-08-08T11:25:30.000000Z	37.8642	29.6617	15	5.9	NM	300	47	-68	Kartal_et_al._(2019)
7234	2019-09-26T10:59:25.000000Z	40.8901	28.1928	12	5.7	RV	281	60	165	Karabulut_et_al._(2020)
7454	2020-01-24T17:55:11.000000Z	38.2987	39.1475	12	6.7	SS	244	68	-8	Taymaz_et_al._(2020)
7824	2020-02-23T05:52:57.000000Z	38.4360	44.4890	15	5.8	NM	328	59	-127	Taymaz_et_al._(2022)
7843	2020-02-23T16:00:29.000000Z	38.4500	44.5020	8	6	SS	294	83	-145	Taymaz_et_al._(2022)
8129	2020-06-14T14:24:27.000000Z	39.3650	40.7140	8	5.9	SS	262	82	160	Sözbilir_et_al._(2020)
8132	2020-06-15T06:51:29.000000Z	39.3678	40.7435	7	5.5	SS	271	82	174	Sözbilir_et_al._(2020)
8262	2020-10-30T11:51:24.000000Z	37.8790	26.7030	15	7	NM	276	37	-90	Ganas_et_al._(2021)
8478	2021-03-03T10:16:10.000000Z	39.8055	22.2578	3	6.3	NM	317	30	-110	Papadopoulos_et_al._(2021)
8652	2021-09-27T06:17:23.000000Z	35.3871	25.3501	10	6	NM	216	53	-95	Triantafyllou_et_al._(2022)

APPENDIX 2 – SMD-TR Example of Event Information

EQID	EQCode	EQ_Lat	EQ_Lon	Depth (km)	Mag	EQ_Type	SoF	Strike P1	Dip P1	Rake P1	Strike P2	Dip P2	Rake P2	RDL (km)	RW (km)	Ztor (km)
1	197608190112	37.7510	29.0120	15	5.3	ACR_shallow	NM	164	45	-30	-999	-999	-999	5.9	5.2	13.2
2	197710050534	41.1130	33.6480	15	5.8	ACR_shallow	SS	76	90	173	-999	-999	-999	10.6	6.4	11.8
3	197712091553	38.3210	27.2170	15	5.2	NA	NA	-999	-999	-999	-999	-999	-999	-999	-999	-999
4	197712160737	38.3790	27.2040	15	5.5	ACR_shallow	NM	304	70	-76	-999	-999	-999	7.4	6.1	12.1
5	197809211937	37.9740	38.5950	15	4.9	NA	NA	-999	-999	-999	-999	-999	-999	-999	-999	-999
6	197904111214	39.0900	43.9210	15	5.2	NA	NA	-999	-999	-999	-999	-999	-999	-999	-999	-999
7	197905280927	36.3800	31.8030	95	5.9	SZ_intraslab	NM	274	71	-71	-999	-999	-999	11.7	8.4	91
8	197907181312	39.6500	28.6710	10	5.3	ACR_shallow	NM	285	56	-93	-999	-999	-999	5.9	5.2	7.8
9	198106300759	36.1390	35.9310	16	5.2	NA	NA	-999	-999	-999	-999	-999	-999	-999	-999	-999
10	198307051201	40.3230	27.2660	15	6.1	ACR_shallow	SS	254	49	-173	-999	-999	-999	16.3	7.7	12.1
11	198310300412	40.3500	42.1940	15	6.6	ACR_shallow	SS	38	73	-17	-999	-999	-999	43.5	17	0
12	198403290006	39.7121	27.9176	11	4.9	ACR_shallow	SS	78.68	84.88	163.9	170.16	73.97	5.33	2.9	3.7	9.2
13	198406170748	38.8330	25.6990	12	5.1	ACR_shallow	SS	249	82	-163	-999	-999	-999	3.9	4.1	10
14	198508120254	40.0220	39.7680	15	5.3	NA	NA	-999	-999	-999	-999	-999	-999	-999	-999	-999
15	198512062235	36.9900	28.8910	15	5.1	NA	NA	-999	-999	-999	-999	-999	-999	-999	-999	-999
16	198605050335	38.0370	37.7700	10	6.1	ACR_shallow	RV	273	49	31	-999	-999	-999	13.1	7.8	7.1
17	198606010643	37.9785	27.3976	10	4.2	NA	NA	-999	-999	-999	-999	-999	-999	-999	-999	-999
18	198606061039	38.0490	37.9020	10	5.9	ACR_shallow	RV	275	27	30	-999	-999	-999	10	6.4	8.5
19	198804200350	39.0420	44.1450	12	5.5	ACR_shallow	SS	110	58	163	-999	-999	-999	6.9	5.3	9.7
20	198808040825	38.8625	26.9388	12	4.8	NA	NA	-999	-999	-999	-999	-999	-999	-999	-999	-999
...	...	...	...	...	...	...	...	...	...	...	...	...	...	...	...	...
9229	202302170011	38.8750	38.1310	12	4	ACR_shallow	NM	12	63	-114	237	35	-51	1.3	1.8	11.2
9230	202302170035	39.1540	40.1720	12	4.8	ACR_shallow	SS	215	84	11	124	79	174	2.5	3.4	10.3
9231	202302170049	37.5220	37.2160	7	4	ACR_shallow	RV	218	36	84	45	54	94	0.8	1.1	6.7
9232	202302170606	38.2570	38.1920	7	4.1	ACR_shallow	SS	82	64	-20	181	72	-153	0.9	2.2	6
9233	202302190056	38.0910	36.2240	13	4.4	ACR_shallow	RV	152	50	73	358	43	109	1.4	1.6	12.4
9234	202302190359	37.2500	36.8250	10	4.3	ACR_shallow	NM	169	62	-122	43	42	-45	1.9	2.3	9
9235	202302190407	37.2360	36.8350	5	4.5	ACR_shallow	NM	180	35	-123	38	61	-69	2.3	2.7	4.2
9236	202302200037	38.7060	39.9890	12	4.7	ACR_shallow	SS	243	57	2	152	89	147	2.2	3.2	10.6
9237	202302200039	38.7020	39.9620	13	4.8	ACR_shallow	SS	341	77	-156	246	67	-14	2.5	3.4	11.3
9238	202302200107	38.6920	39.9630	15	4.6	ACR_shallow	SS	255	76	17	161	74	165	1.9	3	13.5
9239	202302200148	38.0860	36.8120	7	4.5	ACR_shallow	RV	81	80	98	220	13	49	1.5	1.7	6.2
9240	202302200229	38.7180	39.9890	7	4.4	ACR_shallow	SS	242	74	-10	335	81	-164	1.4	2.7	5.7
9241	202302200345	38.6820	40.0010	7	4.5	ACR_shallow	SS	251	69	2	160	88	159	1.7	2.9	5.7
9242	202302201704	36.0370	36.0210	22	6.3	ACR_shallow	NM	225	53	-27	-999	-999	-999	18.6	11.6	17.4
9243	202302201714	36.2540	35.9920	7	4	NA	NA	-999	-999	-999	-999	-999	-999	-999	-999	-999
9244	202302201900	36.1710	36.0430	7	4.2	NA	NA	-999	-999	-999	-999	-999	-999	-999	-999	-999
9245	202302201909	36.2670	36.0520	11	4.1	NA	NA	-999	-999	-999	-999	-999	-999	-999	-999	-999
9246	202302202256	36.1340	35.9540	7	4.2	NA	NA	-999	-999	-999	-999	-999	-999	-999	-999	-999
9247	202302202321	38.0330	37.3860	8	4.4	ACR_shallow	NM	163	40	-74	322	52	-103	2.1	2.5	7.2
9248	202302220709	38.5050	40.2840	10	4.4	ACR_shallow	SS	147	77	-160	52	70	-14	1.4	2.7	8.7

APPENDIX 3 – SMD-TR Example of Record Distance Metrics

WFID	Repi (km)	Rhyp (km)	RJB (km)	Rrup (km)	Rxx (km)	Ryy (km)	Hanging Wall Flag
1	7.2	17	5.3	14	-5.3	0	FW
2	72	74	67	68	16	65	FW
3	14	21	-999	-999	-999	-999	NA
4	11	18	7	14	-3.5	6.1	FW
5	47	50	-999	-999	-999	-999	NA
6	17	23	-999	-999	-999	-999	NA
7	161	187	156	183	114	109	FW
8	6.4	12	4.5	9	-4.5	0	FW
9	22	27	-999	-999	-999	-999	NA
10	84	86	78	79	-70	35	FW
11	40	42	33	35	-28.6	16	FW
12	51	53	42	44	-8.7	41	FW
13	73	75	67	69	65	30	HW
14	93	94	88	89	-85.2	23	FW
15	34	37	20	24	24	6.4	HW
16	94	95	72	72	-28.3	66	FW
17	8.4	14	8.4	14	5.8	4.2	HW
18	93	94	91	92	-49.1	77	FW
19	88	89	-999	-999	-999	-999	NA
20	18	24	-999	-999	-999	-999	NA
...	...	...	...	...	...	...	...
95876	142	142	142	142	-95	103	FW
95877	131	132	131	132	-75	81	FW
95878	146	147	146	147	-94	102	FW
95879	137	138	137	138	-89	96	FW
95880	128	128	128	128	36	78	UD
95881	134	134	134	134	22	87	UD
95882	137	137	137	137	83	90	UD
95883	153	154	153	154	70	76	UD
95884	149	150	149	150	95	103	UD
95885	132	132	132	132	-32	82	FW
95886	125	126	125	126	-61	66	FW
95887	91	91	91	91	-35	49	FW
95888	134	134	134	134	-28	85	FW
95889	133	133	133	133	-53	71	FW
95890	149	149	149	149	100	108	FW
95891	118	119	118	119	65	70	UD
95892	103	104	103	104	38	58	UD
95893	142	142	142	142	59	76	UD
95894	112	113	112	113	13	74	FW
95895	99	99	99	99	0.8	66	FW

APPENDIX 4 – SMD-TR Example of Record Processing Information

WFID	Preferred Source	Usable Period (s)	Component 1 Low-cut Frequency (Hz)	Component 2 Low-cut Frequency (Hz)	Component 3 Low-cut Frequency (Hz)	Component 1 High-cut Frequency (Hz)	Component 2 High-cut Frequency (Hz)	Component 3 High-cut Frequency (Hz)
1	Akkar_et_al_2014	1	0.7	0.5	0.6	35	50	35
2	APAR	-1	-999	-999	-999	-999	-999	-999
3	APAR	-1	-999	-999	-999	-999	-999	-999
4	Akkar_et_al_2014	1.3	0.5	0.5	0.5	25	25	25
5	APAR	-1	-999	-999	-999	-999	-999	-999
6	APAR	-1	-999	-999	-999	-999	-999	-999
7	Akkar_et_al_2014	0.6	1.2	1.2	1.2	40	100	100
8	Akkar_et_al_2014	2	0.35	0.3	0.7	30	30	40
9	Akkar_et_al_2014	4	0.2	0.1	0.1	15	20	20
10	APAR	-1	0.0244	-999	-999	44.2	-999	-999
11	Akkar_et_al_2014	7	0.1	0.1	-999	25	25	-999
12	Akkar_et_al_2014	1.8	0.4	0.25	0.3	25	25	30
13	APAR	-1	-999	-999	-999	-999	-999	-999
14	APAR	-1	-999	-999	-999	-999	-999	-999
15	Akkar_et_al_2014	4.7	0.03	0.15	0.12	100	85	8
16	APAR	-1	-999	-999	-999	-999	-999	-999
17	APAR	-1	-999	-999	-999	-999	-999	-999
18	APAR	-1	-999	-999	-999	-999	-999	-999
19	APAR	-1	-999	-999	-999	-999	-999	-999
20	APAR	-1	-999	-999	-999	-999	-999	-999
...	...	...	...	...	...	...	...	...
95876	APAR	-1	-999	-999	-999	-999	-999	-999
95877	APAR	-1	-999	-999	-999	-999	-999	-999
95878	APAR	-1	-999	-999	-999	-999	-999	-999
95879	APAR	4.9	0.1587	0.1648	0.2014	47.5	47.6	48.6
95880	APAR	3	0.2014	0.2624	0.3418	28.4	18	18.1
95881	APAR	-1	-999	-999	-999	-999	-999	-999
95882	APAR	5.5	0.1465	0.0488	0.1038	33.8	32.5	31.9
95883	APAR	-1	-999	-999	-999	-999	-999	-999
95884	APAR	-1	-999	-999	-999	-999	-999	-999
95885	APAR	8.7	0.0915	0.0793	0.1343	29.7	29.9	28.1
95886	APAR	-1	-999	-999	-999	-999	-999	-999
95887	APAR	1.8	0.4333	0.0915	0.2319	17.4	13.8	17.9
95888	APAR	-1	-999	-999	-999	-999	-999	-999
95889	APAR	-1	-999	-999	-999	-999	-999	-999
95890	APAR	4.9	0.1648	0.1282	0.2014	28.5	29	27
95891	APAR	-1	-999	-999	-999	-999	-999	-999
95892	APAR	8.7	0.0915	0.0915	0.1404	37.9	32.8	38.7
95893	APAR	-1	-999	-999	-999	-999	-999	-999
95894	APAR	-1	-999	-999	-999	-999	-999	-999
95895	APAR	-1	-999	-999	-999	-999	-999	-999

APPENDIX 5 – SMD-TR Example of Station Information

Station Code	Network	Province	District	Station Latitude	Station Longitude	Vs30 (m/s)	Z1 (m)
101	TK	Adana	Çukurova	37.0440	35.2260	478	95
102	TK	Adana	Sarıçam	37.0579	35.3670	417	78
103	TK	Adana	Yüreğir	36.9958	35.3706	423	59
104	TK	Adana	Ceyhan	37.0240	35.8095	223	-999
105	TK	Adana	Ceyhan	37.0267	35.8162	263	-999
106	TK	Adana	Yüreğir	36.9080	35.5670	210	-999
107	TK	Adana	Sarıçam	37.0330	35.6330	405	-999
108	TK	Adana	Yüreğir	36.8760	35.6170	654	35
109	TK	Adana	Ceyhan	37.1780	35.6890	253	-999
110	TK	Adana	Karataş	36.5680	35.3901	486	31
111	TK	Adana	Seyhan	37.0185	35.2254	461	-999
112	TK	Adana	Yüreğir	36.8716	35.4763	490	150
113	TK	Adana	Yüreğir	36.9555	35.6273	267	-999
114	TK	Adana	Ceyhan	37.1758	35.6929	483	-999
115	TK	Adana	Sarıçam	37.0812	35.4544	322	-999
116	TK	Adana	Sarıçam	37.1047	35.4626	466	-999
117	TK	Adana	Yüreğir	36.8384	35.2411	215	-999
118	TK	Adana	Çukurova	37.0362	35.3184	946	12
119	TK	Adana	Karataş	36.5680	35.3900	485	-999
120	TK	Adana	Yumurtalık	36.7701	35.7901	439	-999
...	...	...	...	...	...	...	...
UMTK	GZ	Ankara	Çankaya	39.8862	32.6916	300	-999
GAZI	TU	Antalya	Gazipaşa	36.2347	32.3157	-1	-999
KORT	TU	Antalya	Korkuteli	37.0007	30.3503	1822	-999
BLKS	TU	Balıkesir	Karesi	39.8745	27.9684	-1	-999
MNGN	GZ	Bolu	Mengen	40.9386	32.0741	-1	-999
IMRA	TU	Bursa	Karacabey	40.5639	28.5285	-1	-999
BOZC	TU	Çanakkale	Bozcaada	39.8417	26.0528	1005	-999
CNKL	TU	Çanakkale	Çanakkale_Merkez	40.0662	26.3872	-1	-999
ILGZ	GZ	Çankırı	Ilgaz	40.9248	33.6282	-1	-999
DNZT	TU	Denizli	Tavas	37.2787	29.0248	-1	-999
EKAR	TU	Erzurum	Karaçoban	39.2559	42.0640	445	-999
BORA	TU	Eskişehir	Tepebaşı	39.8801	30.4534	630	-999
YAYL	TU	Hatay	Yayladağı	36.0343	36.1070	1011	-999
IZMD	TU	İzmir	Dikili	38.9842	26.9281	-1	-999
IZMR	TU	İzmir	Ödemiş	38.1367	27.9522	-1	-999
KHMR	TU	Kahramanmaraş	Türkoğlu	37.3439	36.9080	-1	-999
NAR	TU	Kahramanmaraş	Pazarcık	37.3919	37.1574	-1	-999
BDRM	TU	Muğla	Bodrum	37.0653	27.4442	1040	-999
SINO	TU	Sinop	Sinop_Merkez	42.0184	35.2019	581	-999
KURT	TU	Yalova	Yalova_Merkez	40.5905	29.2092	-1	-999

APPENDIX 6 – SMD-TR Example of PSA Values at 111 Periods

WFID	PGA East-West Component (g)	PGV East-West Component (cm/s)	PGD East-West Component (cm)	T0.010s (g)	T0.020s (g)	T0.022s - T14.00s (g)	T15.000s (g)	T20.000s (g)
1	0.2702	16.75	1.31	2.74E-01	2.90E-01	…	2.30E-04	1.30E-04
4	0.1301	4.98	0.23	1.31E-01	1.33E-01	…	4.27E-05	2.39E-05
7	0.0136	0.49	0.08	1.88E-02	1.93E-02	…	9.01E-06	5.09E-06
8	0.2754	8.57	0.91	2.79E-01	2.88E-01	…	1.62E-04	9.13E-05
9	0.1213	7.24	1.15	1.22E-01	1.23E-01	…	2.59E-04	1.46E-04
10	0.0230	1.33	0.50	2.32E-02	2.54E-02	…	9.97E-05	4.97E-05
11	0.0448	3.03	0.76	4.51E-02	4.57E-02	…	2.00E-04	1.05E-04
12	0.0476	2.34	0.23	4.78E-02	4.81E-02	…	4.24E-05	2.37E-05
15	0.1757	29.56	21.29	1.82E-01	1.81E-01	…	6.44E-03	2.76E-03
21	0.0778	6.64	2.05	7.79E-02	7.82E-02	…	4.55E-04	2.47E-04
23	0.0329	4.02	1.64	3.30E-02	3.32E-02	…	3.13E-04	1.73E-04
28	0.0290	2.12	0.48	2.91E-02	2.93E-02	…	9.20E-05	5.04E-05
29	0.4836	77.48	36.27	4.87E-01	5.15E-01	…	5.85E-03	3.42E-03
30	0.0302	7.56	6.32	3.03E-02	3.03E-02	…	1.45E-03	6.98E-04
31	0.0822	3.21	1.13	8.24E-02	8.33E-02	…	2.14E-04	1.09E-04
32	0.0398	4.71	1.61	3.99E-02	3.99E-02	…	3.17E-04	1.87E-04
33	0.0710	3.96	0.84	7.21E-02	7.62E-02	…	2.22E-04	1.20E-04
35	0.0331	4.52	1.33	3.32E-02	3.33E-02	…	3.52E-04	1.88E-04
61	0.0958	3.68	0.28	9.64E-02	9.73E-02	…	5.07E-05	2.87E-05
73	0.0486	3.69	0.60	4.87E-02	4.87E-02	…	1.12E-04	6.11E-05
…	…	…	…	…	…	…	…	…
95859	0.0049	0.14	0.01	4.96E-03	5.02E-03	…	2.19E-06	1.25E-06
95860	0.0012	0.07	0.01	1.24E-03	1.25E-03	…	1.20E-06	6.59E-07
95861	0.0002	0.01	0.00	1.96E-04	1.97E-04	…	2.62E-07	1.47E-07
95862	0.0011	0.05	0.00	1.07E-03	1.08E-03	…	7.43E-07	4.30E-07
95863	0.0041	0.18	0.01	4.14E-03	4.17E-03	…	2.42E-06	1.40E-06
95865	0.0011	0.05	0.01	1.11E-03	1.14E-03	…	1.11E-06	6.11E-07
95866	0.0008	0.04	0.01	8.33E-04	8.67E-04	…	1.82E-06	1.00E-06
95868	0.0044	0.25	0.02	4.38E-03	4.42E-03	…	3.94E-06	2.24E-06
95869	0.0006	0.03	0.01	6.45E-04	6.50E-04	…	1.04E-06	5.68E-07
95871	0.0008	0.03	0.00	8.19E-04	8.49E-04	…	4.98E-07	2.74E-07
95872	0.0038	0.15	0.02	3.87E-03	3.92E-03	…	3.00E-06	1.49E-06
95873	0.0019	0.16	0.02	1.88E-03	1.88E-03	…	2.72E-06	1.49E-06
95874	0.0001	0.00	0.00	6.24E-05	9.21E-05	…	8.90E-08	5.01E-08
95879	0.0003	0.02	0.00	3.00E-04	3.50E-04	…	3.68E-07	2.07E-07
95880	0.0002	0.01	0.00	2.49E-04	2.51E-04	…	2.78E-07	1.51E-07
95882	0.0012	0.04	0.00	1.23E-03	1.25E-03	…	5.86E-07	3.30E-07
95885	0.0006	0.04	0.01	5.95E-04	5.99E-04	…	1.84E-06	8.40E-07
95887	0.0003	0.02	0.00	2.78E-04	2.79E-04	…	3.44E-07	1.95E-07
95890	0.0006	0.02	0.00	5.53E-04	5.59E-04	…	2.94E-07	1.59E-07
95892	0.0016	0.05	0.00	1.67E-03	1.74E-03	…	9.36E-07	4.66E-07

APPENDIX 7 – SMD-TR Example of Intensity Measures

WFID	ARIAS Intensity of East-West Component (m/s)	CAV of East-West Component (cm/s)	Significant Duration of 5-75% for East-West Component (s)	Significant Duration of 5-95% for East-West Component (s)	Significant Duration of 20-80% for East-West Component (s)
1	5.22E-01	39.91	2.08	5.83	1.97
4	6.42E-02	9.09	0.53	2.02	0.40
7	4.52E-04	0.61	0.87	1.29	0.86
8	2.09E-01	19.36	1.18	2.49	0.85
9	1.76E-01	41.48	6.42	19.16	6.10
10	5.07E-03	4.47	5.05	9.36	4.98
11	2.87E-02	11.11	5.38	8.61	2.73
12	2.29E-02	10.58	5.63	9.44	3.83
15	4.12E-01	60.88	12.81	18.39	13.20
21	4.65E-02	15.94	5.76	10.61	4.53
23	1.57E-02	8.09	4.38	8.44	2.91
28	1.00E-02	7.12	6.77	9.91	6.97
29	1.76E+00	90.16	2.10	9.77	2.72
30	2.70E-02	13.90	12.27	16.86	7.82
31	5.68E-02	15.54	6.44	9.50	3.01
32	2.10E-02	12.91	5.74	17.89	6.86
33	9.32E-02	23.16	6.00	9.96	5.48
35	2.30E-02	13.84	10.19	18.37	10.82
61	4.86E-02	10.30	1.82	4.31	1.38
73	3.27E-02	12.93	7.39	9.96	5.05
…	…	…	…	…	…
95859	1.62E-04	0.92	2.43	6.69	1.40
95860	1.73E-05	0.46	12.32	18.81	5.84
95861	1.13E-06	0.14	17.94	28.42	9.73
95862	1.19E-05	0.36	7.53	15.72	5.18
95863	1.91E-04	1.24	5.27	12.92	5.31
95865	3.08E-05	0.75	17.97	36.37	13.42
95866	1.34E-05	0.51	16.18	56.79	16.95
95868	2.27E-04	1.26	6.57	11.01	4.14
95869	8.37E-06	0.39	18.36	33.54	12.07
95871	8.81E-06	0.34	12.70	22.09	8.16
95872	9.02E-05	0.77	3.86	8.95	3.12
95873	5.16E-05	0.69	6.13	15.19	4.14
95874	1.36E-07	0.06	23.55	62.52	23.93
95879	1.76E-06	0.19	19.25	34.45	12.86
95880	1.03E-06	0.13	17.00	30.26	6.19
95882	2.02E-05	0.49	8.27	17.84	5.36
95885	9.00E-06	0.42	18.59	38.95	9.76
95887	1.91E-06	0.18	16.33	31.91	11.47
95890	8.63E-06	0.44	22.66	34.75	23.25
95892	2.56E-05	0.60	10.46	27.61	4.35